

Enhancement of non-Gaussianity and nonclassicality of pair coherent states with postselected von Neumann measurement

Yi-Fang Ren^{1§}, Janarbek Yuanbek^{1§}, and Yusuf Turek^{1*}

¹*School of Physics, Liaoning University, Shenyang, Liaoning 110036, China*

(Dated: May 13, 2025)

We investigate the effects of postselected von Neumann measurements on the nonclassical properties of pair coherent states (PCS). We calculated key quantum characteristics, such as squeezing, photon statistics, entanglement between the two PCS modes, and teleportation fidelity. Our results demonstrate that postselected von Neumann measurements enhance both the non-Gaussianity and nonclassicality of PCS. These findings are validated by analyzing the scaled joint Wigner function across various system parameters. We also notice that in weak measurement regimes, the teleportation fidelity via a PCS-based quantum channel under postselected von Neumann measurements could keep successful teleportation for anomalous weak values of the system observable. The theoretical optimization scheme offers an alternative approach for improving PCS-based quantum information efficiency and facilitates practical implementations in quantum technologies.

I. INTRODUCTION

The nonclassicality of quantum states plays a crucial role in quantum computation and information processing. Recent advancements in technology allow the manipulation of photons, making continuous-variable states of bosonic modes an excellent platform for quantum information processing. Among the variety of continuous-variable states [1–3], two-mode Gaussian and non-Gaussian states such as entangled cat states [4], N0ON states [5, 6], squeezed states [7, 8], and pair coherent states (PCS) [9] have irreplaceable roles in numerous applications [10–18]. In two-mode nonclassical states, enhancing nonclassicality and entanglement properties can be achieved through photon addition and subtraction operations [19–31]. However, operating with non-Gaussian states introduces additional computational complexity compared to Gaussian states. Beyond photon addition and subtraction (or their superpositions) [32], quantum catalysis provides another feasible method for enhancing the nonclassicality of quantum states [29]. Quantum catalysis enhances quantum properties without directly altering the photon count. This enhancement arises from the inherently quantum mechanical nature of the process (for further details, refer to [33], and references therein). However, quantum catalysis is not universally applicable to all states, necessitating alternative methods for optimizing nonclassical states. Specifically, exploring new state-optimization schemes is essential for improving the efficiency of multimode state-based applications—such as multimode Gaussian and non-Gaussian states—without relying on photon addition or subtraction operations.

The process of optimizing quantum states relates to the measurement problems. It requires modifying and effectively manipulating measurement procedures to enhance

the properties of a given state using quantum control techniques [34]. Quantum weak measurements (WMs) [35], a novel class of generalized measurement methods, offer feasible and effective pathways for optimizing quantum states for specific tasks. Unlike the strong measurements, WMs involve a weak coupling between the measured system and the measuring device, which prevents the destruction of the system's initial state. While a single trial of a WM does not yield precise information about the system, repeated measurements combined with postselection allow for the statistical extraction of desired observable information. The extracted weak value is a complex quantity that can lie outside the eigenvalue spectrum of the observable [36, 37]. This phenomenon, known as weak value amplification (WVA), is useful for amplifying weak signals in quantum systems [38] (for further insights into WM theory and its applications, readers may consult the works of Nori [39] and Boyd [40]). The utility of quantum WM techniques in state preparation [41] and optimization processes has been demonstrated for various quantum states and optimization processes has been demonstrated for various quantum states [42, 43]. However, their advantages for multimode continuous-variable states of bosonic modes remain largely unexplored. For instance, while single-mode coherent states are typical semiclassical states that minimize (and equalize) the uncertainty product of two incompatible operators, PCS serve as two-mode analogs of Glauber coherent states. PCS are eigenstates of the pair-photon annihilation operator and represent a promising candidate for applying quantum WM-based state optimization methods.

In this work, we investigate how the properties of PCS change after applying the theory of postselected measurements to one mode of PCS. We calculate the squeezing, quantum statistics, and entanglement characteristics of the measurement output state. Our results show that postselected von Neumann measurements could enhance the non-Gaussianity and nonclassicality of PCS, considering large weak values of the measured system observ-

[§] These authors contributed equally to this work.

* yusuftu1984@hotmail.com

able and appropriate coupling strength parameters between the measured system and measuring device (MD). We confirm these findings by examining the phase-space distribution of our state, characterized by the scaled joint Wigner function. We also check the teleportation fidelity with postselected von Neumann measurements to the PCS and the numerical outcomes indicate that in weak measurement regimes the quantum teleportation task based on PCS-based quantum channel is still could keep its validity for larger weak values of measured system observable.

We organized the paper as follows: In Sec. II, we present our theoretical model. Section III explores the effects of postselection on the squeezing properties of PCS, including quadrature and sum squeezing. In Sec. IV, we investigate the quantum statistics of postselected PCS under von Neumann measurements, analyzing the relationship between the a mode and b mode using the second-order cross-correlation (SOCC) and second-order correlation functions. Section V examines entanglement through measures such as the Hillery-Zubairy (HZ) correlation and Einstein-Podolsky-Rosen (EPR) correlation. In Sec. VI, we investigate the scaled joint Wigner function of our measurement output state and take comparison with the initial PCS case. Section VII we present the state distance between initial and final MD states, and give the details of the teleportation fidelity of a coherent state transmitted through a PCS-based quantum channel under postselected von Neumann measurements. Finally, Sects. VIII and IX present a discussion and conclusion, respectively. Throughout this paper, we take $\hbar = 1$.

II. MODEL SETUP

The coherent state is a typical semi-classical state that minimizes (and equalizes) the uncertainty product of two incompatible operators. However, the Gaussian profile characterizing the classicality of coherent states transforms into a non-Gaussian profile upon the addition of a single photon. Beyond the standard coherent state and the single-photon-added coherent state, there also exist two-mode entangled coherent states, commonly referred to as PCS [44].

Analogous to the usual coherent state, defined as $|\alpha\rangle = e^{-|\alpha|^2/2} \sum_n \alpha^n / \sqrt{n!} |n\rangle$, the PCS are a superposition of twin-Fock state bases $|n + \delta\rangle_a |n\rangle_b$ of two harmonic oscillators (a and b):

$$|\gamma, \delta\rangle = \mathcal{N}_\delta \sum_{n=0}^{\infty} \frac{\gamma^{n+\delta/2}}{\sqrt{n!(n+\delta)!}} |n + \delta\rangle_a |n\rangle_b. \quad (1)$$

Here, γ is a complex number representing the amplitude and phase of the state, δ is an integer denoting the photon number difference (PND) between the two modes; and \mathcal{N}_δ is a normalization coefficient defined by:

$$\mathcal{N}_\delta = \left(\sum_{n=0}^{\infty} \frac{|\gamma|^{2n+\delta}}{n!(n+\delta)!} \right)^{-\frac{1}{2}} = \frac{1}{\sqrt{I_\delta(2|\gamma|)}}. \quad (2)$$

Here, $I_\delta(2|\gamma|)$ denotes the modified Bessel function of the first kind, expressed as follows:

$$I_\delta(x) = \sum_{n=0}^{\infty} \frac{1}{n!(n+\delta)!} \left(\frac{x}{2} \right)^{2n+\delta}. \quad (3)$$

This state is an eigenstate of the pair-photon annihilation operator ab and the PND operator $a^\dagger a - b^\dagger b$:

$$ab|\gamma, \delta\rangle = \gamma|\gamma, \delta\rangle, \quad (4)$$

$$(a^\dagger a - b^\dagger b)|\gamma, \delta\rangle = \delta|\gamma, \delta\rangle. \quad (5)$$

Here, a (a^\dagger) and b (b^\dagger) are the annihilation (creation) operators associated with the two modes (a mode and b mode) of the PCS, respectively. The various generation methods have been proposed theoretically in different physical systems [9, 45–49]. The generation and characterization of PCS within spatially two confined superconducting cavities have been explored in recent experimental work [50]. As indicated in previous theoretical [46] and experimental [51] works, it also may possible to generate and manipulate of PCS in trapped ions systems. In order to facilitate the PCS in long-distance quantum information processing and communication tasks in most recent work [52] the experimentally feasible theoretical proposal to the generation of PCS in open space with high fidelity also introduced in detail. PCS are a type of two-mode non-Gaussian and nonclassical states [20], and its sub-Poissonian statistics, correlations in number fluctuations, squeezing, and violations of Cauchy-Schwarz inequalities (CSI) have been studied extensively [28, 30, 44, 53, 54]. As non-Gaussian entangled states, PCS offers advantages in performing quantum tasks such as quantum communication [10, 55, 56], interferometric lithography [57], quantum metrology [58], quantum dialogue [59] and quantum key distribution [12, 15].

To study the effects of postselected von Neumann measurement on the PCS, we consider the PCS as the MD and its polarization as the measured system. As illustrated in Fig. 1, we simplify the setup by restricting the interaction between the MD and the measured system to the a -mode. The interaction Hamiltonian H_{int} is of the von Neumann type, expressed as:

$$H_{int} = g\sigma_x \otimes P_x. \quad (6)$$

Here, g denotes the interaction strength between the MD and the measured system. The operator $\sigma_x = |D\rangle\langle D| - |A\rangle\langle A|$ represents the observable of the measured system, where $|D\rangle = \frac{1}{\sqrt{2}} (|H\rangle + |V\rangle)$, and $|A\rangle = \frac{1}{\sqrt{2}} (|H\rangle - |V\rangle)$ correspond to the diagonal and anti-diagonal polarizations of the beam, respectively. Here, $|H\rangle$ and $|V\rangle$ denote

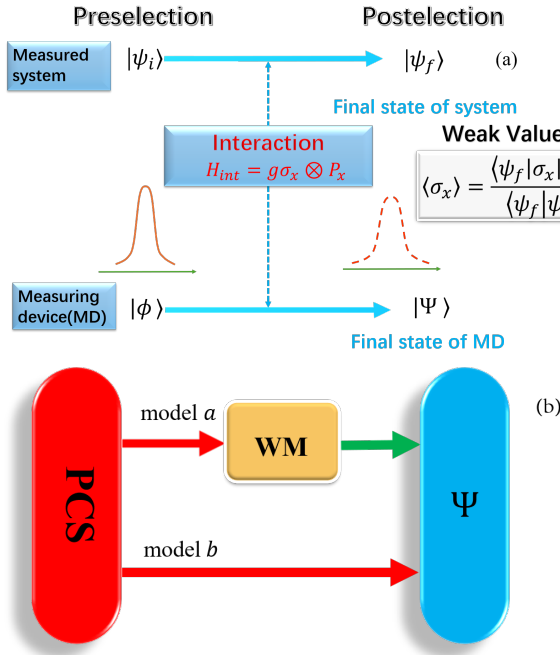


Figure 1. (a) Schematic diagram of weak measurement (WM) theory. The standard process of WM involves four steps: 1. *Preparation*: The initial state of the measured system is prepared as $|\psi_i\rangle$, while the MD is initialized in the state $|\phi\rangle$. 2. *Weak Interaction*: A weak interaction occurs between the measured system and the MD, during which the composite system evolves according to the Hamiltonian $H_{int} = g\sigma_x \otimes P_x$. Here, the coupling constant g characterizes the bilinear coupling. 3. *Postselection*: After evolution, the entire system is projected onto the postselected state $|\psi_f\rangle$. This step extracts the desired observable values of the system by selecting a specific subensemble of samples before the final measurement. 4. *Readout*: The measurement result determines the shifts in the MD. In the postselected weak measurement process, the observable value is a function of the weak value. The real (Re) and imaginary (Im) parts of the weak value are derived from the shifts in the canonical position and momentum of the MD respectively. (b) Schematic setup for preparing $|\Psi\rangle$ via postselected von Neumann measurement. Experimentally, the pointer is initially in the PCS. Using the WM strategy, where the interaction is restricted to the a -mode, we investigate the effects of this measurement on the properties of the PCS.

the horizontal and vertical polarizations of photons. In the interaction Hamiltonian, P_x represents the canonical momentum of the MD and can be expressed in terms of annihilation and creation operators as follows:

$$P_x = \frac{i}{2\sigma} (a^\dagger - a), \quad (7)$$

where $\sigma = \sqrt{1/2m\omega}$ represents the beam width. We now assume that the composite system is initially prepared in the following form:

$$|\Psi_{in}\rangle = |\psi_i\rangle \otimes |\phi\rangle, \quad (8)$$

where $|\psi_i\rangle = \cos \frac{\alpha}{2} |H\rangle + e^{i\vartheta} \sin \frac{\alpha}{2} |V\rangle$ and $|\phi\rangle = |\gamma, \delta\rangle$. As shown in Fig. 1, $|\psi_i\rangle$ and $|\phi\rangle$ represent the states of the measured system and the MD, respectively. The initial state is thus the product state between the measured system and the MD. Here, $\vartheta \in [0, 2\pi]$ and $\alpha \in [0, \pi)$. Experimentally, this type of initial state can be prepared by passing the beam through a quarter-wave and half-wave plates with appropriate optical axis angles. The joint state, expressed in Eq. (8), evolves over time under the influence of the time evolution operator $U(t) = \exp\left(-i \int_0^t H_{int} d\tau\right)$, as follows:

$$\begin{aligned} |\Psi_{evol}\rangle &= \exp\left(-i \int_0^t H_{int} d\tau\right) |\Psi_{in}\rangle \\ &= \frac{1}{2} \left[(\mathbb{I} + \sigma_x) D\left(\frac{\Gamma}{2}\right) + (\mathbb{I} - \sigma_x) D^\dagger\left(\frac{\Gamma}{2}\right) \right] (9) \\ &\times |\psi_i\rangle \otimes |\phi\rangle, \end{aligned}$$

where $\Gamma = gt/\sigma$ represents the ratio between gt and σ , \mathbb{I} is the 2×2 identity matrix, and $D(\Gamma/2) = e^{\frac{\Gamma}{2}(\hat{a}^\dagger - \hat{a})}$ is the displacement operator acting on the a mode of the PCS. It is important to note that the coupling strength parameter Γ characterizes the measurement strength in this study. The coupling between measured system and MD is referred to as weak when $\Gamma \ll 1$ and strong when $\Gamma \gg 1$. For this reason, Γ can be considered the transaction parameter in our measurement model. The measurement process involves postselection. In this study, we assume the postselection of the system state to be $|\psi_f\rangle = |H\rangle$. After postselecting the system state, the final state of the MD is obtained, and its expression is given as

$$|\Psi\rangle = \frac{\lambda}{2} \left[(1 + \langle\sigma_x\rangle_w) D\left(\frac{\Gamma}{2}\right) + (1 - \langle\sigma_x\rangle_w) D^\dagger\left(\frac{\Gamma}{2}\right) \right] |\phi\rangle. \quad (10)$$

Here, λ is the normalization coefficient given by

$$\lambda = \frac{\sqrt{2}}{[1 + |\langle\sigma_x\rangle_w|^2 + (1 - |\langle\sigma_x\rangle_w|^2)P]^{\frac{1}{2}}}, \quad (11)$$

with $P = \mathcal{N}_\delta^2 e^{-\frac{\Gamma^2}{2}} \sum_{n=0}^{\infty} \left[\frac{|\gamma|^{2n+\delta}}{n!(n+\delta)!} L_{n+\delta}^{(0)}(\Gamma^2) \right]$, and $\langle\sigma_x\rangle_w$ is the weak value of the system observable σ_x defined as

$$\langle\sigma_x\rangle_w = \frac{\langle\psi_f|\sigma_x|\psi_i\rangle}{\langle\psi_f|\psi_i\rangle} = e^{i\vartheta} \tan \frac{\alpha}{2}. \quad (12)$$

For simplification, we assume the weak value to be a real number by setting $\vartheta = 0$. In calculating the normalization

coefficient λ , the following expressions were used

$$\langle n+d|D(\alpha)|n\rangle = \sqrt{\frac{n!}{(n+d)!}} e^{-\frac{|\alpha|^2}{2}} \alpha^d L_n^{(d)}(|\alpha|^2), \quad (13)$$

$$\langle n|D(\alpha)|n+d\rangle = \sqrt{\frac{n!}{(n+d)!}} e^{-\frac{|\alpha|^2}{2}} (-\alpha^*)^d L_n^{(d)}(|\alpha|^2), \quad (14)$$

where d is natural number, and $L_n^{(d)}(|\alpha|^2)$ represents the associated Laguerre polynomials, given by

$$L_n^{(d)}(|\alpha|^2) = \sum_{m=0}^n (-1)^m C_{n+d}^{m+d} \frac{|\alpha|^{2m}}{m!}. \quad (15)$$

We have to mention that in the derivation of final state of MD, i.e., Eq. (10), we don't use any approximation and the coupling strength parameter Γ can take arbitrary value. If we interested in standard weak measurement regime, its enough to us only consider up to first-order term of the displacement operator $D(\frac{\Gamma}{2})$ since $\Gamma \ll 1$ in this case, i.e., $D(\frac{\Gamma}{2}) \approx 1 + \frac{\Gamma}{2}(a^\dagger - a)$. However, as studied in previous works [60, 61], the weak value $\langle \sigma_x \rangle_w$ in our scheme just a quantity of system observable σ_x induced by particular pre- and post-selection processes on measured system, and it's valid both in Aharonov's weak measurement and von Neumann's projective strong measurement regimes.

Next, we examine the effects of postselected von Neumann measurement and the weak values of the measured system's observable on the inherent properties of the PCS $|\phi\rangle$.

III. THE EFFECTS ON SQUEEZING

In this section, we investigate the effects of postselected von Neumann measurement on the squeezing properties of the PCS by examining both quadrature squeezing and sum squeezing.

A. Quadrature squeezing

In continuous-variable quantum optics, quadrature squeezing is a crucial characteristic of nonclassical radiation fields, playing a vital role in the implementation of various quantum computation and communication protocols [62]. Here, we analyze how postselected von Neumann measurement influences the quadrature squeezing of the PCS.

For a single-mode radiation field, squeezing refers to the reduction of the quadrature variance below the shot noise level, i.e., $\Delta^2 X_\epsilon < \frac{1}{4}$. The quadrature operator with phase ϵ is defined as: $X_\epsilon = \frac{1}{2}(e^{-i\epsilon}a + e^{i\epsilon}a^\dagger)$, where its variance is given by: $\Delta^2 X = \langle X^2 \rangle - \langle X \rangle^2$. Similarly,

for two-mode radiation fields, the quadrature operators can be defined as [63]:

$$F_1 = \frac{1}{2^{3/2}} [e^{-i\epsilon}(a + b) + e^{i\epsilon}(a^\dagger + b^\dagger)], \quad (16)$$

$$F_2 = \frac{1}{2^{3/2}i} [e^{-i\epsilon}(a + b) + e^{i\epsilon}(a^\dagger + b^\dagger)]. \quad (17)$$

They satisfy the commutation relation $[F_1, F_2] = \frac{i}{2}$, and the uncertainty relation for their fluctuations is

$$\Delta^2 F_1 \Delta^2 F_2 \geq \frac{1}{16}, \quad (18)$$

where $\Delta F_i^2 = \langle F_i^2 \rangle - \langle F_i \rangle^2$. Similar to the single-mode case, two-mode squeezing occurs when one of the variances $\Delta^2 F_i$ is below the shot noise level, i.e., $\Delta^2 F_i < 0.25$ ($i = 1, 2$). This condition can be satisfied if the two modes are uncorrelated, with one or both of F_i individually squeezed, or when nonclassical correlations, such as entanglement between the two modes, are present. We use the squeezing parameter to characterize the squeezing of the quadrature as follows:

$$Q_i = \Delta F_i^2 - \frac{1}{4}. \quad (19)$$

As we can see, the values of Q_i are bounded as $Q_i \geq -\frac{1}{4}$, and the i -th component of the quadrature operators of the PCS is said to be squeezed if $-\frac{1}{4} \leq Q_i < 0$. After some algebra, we can obtain the specific expressions for the quadrature squeezing parameter Q_i of the final MD state $|\Psi\rangle$, expressed as:

$$\begin{aligned} Q_{1,\Psi} = & \frac{1}{4} [\langle a^\dagger a \rangle + \langle b^\dagger b \rangle + \text{Re} [\langle a^2 \rangle] + \text{Re} [\langle b^2 \rangle]] \\ & + \frac{1}{2} [\text{Re} [\langle ab \rangle] + \text{Re} [\langle a^\dagger b \rangle]] \\ & - \frac{1}{2} [\text{Re} [\langle a \rangle] + \text{Re} [\langle b \rangle]]^2, \end{aligned} \quad (20)$$

and

$$\begin{aligned} Q_{2,\Psi} = & \frac{1}{4} [\langle a^\dagger a \rangle + \langle b^\dagger b \rangle + \text{Re} [\langle a^2 \rangle] + \text{Re} [\langle b^2 \rangle]] \\ & - \frac{1}{2} [\text{Re} [\langle ab \rangle] - \text{Re} [\langle a^\dagger b \rangle]] \\ & - \frac{1}{2} [\text{Im} [\langle a \rangle] + \text{Im} [\langle b \rangle]]^2. \end{aligned} \quad (21)$$

Here, $\langle \dots \rangle$ represents the expectation value of the associated operators under the the final MD state $|\Psi\rangle$, while Re and Im denote its real and imaginary parts. Additionally, we set $\epsilon = 0$. The Appendix A provides analytic expressions for the expectation values of the associated operators. If we set $\Gamma = 0$, the above two expressions reduce to $Q_{1,\phi}$ and $Q_{2,\phi}$, corresponding to the

initial MD state $|\phi\rangle$ defined in Eq. (1), and expressed as

$$Q_{1,\phi} = \frac{1}{4} \left(\frac{|\gamma| I_{\delta-1}(2|\gamma|)}{I_{\delta}(2|\gamma|)} + \frac{|\gamma| I_{\delta+1}(2|\gamma|)}{I_{\delta}(2|\gamma|)} + 2\text{Re}[\gamma] \right), \quad (22)$$

and

$$Q_{2,\phi} = \frac{1}{4} \left(\frac{|\gamma| I_{\delta-1}(2|\gamma|)}{I_{\delta}(2|\gamma|)} + \frac{|\gamma| I_{\delta+1}(2|\gamma|)}{I_{\delta}(2|\gamma|)} - 2\text{Re}[\gamma] \right), \quad (23)$$

Here, $I_{\delta}(2|\gamma|)$ is the modified Bessel function defined in Eq. (3). From $Q_{1,\phi}$, we can deduce that $Q_{1,\phi} \geq 0$ for all γ , indicating that the F_1 quadrature of initial PCS $|\phi\rangle$ never exhibits squeezing. Furthermore, if the third term, $2\text{Re}[\gamma]$, in $Q_{2,\phi}$ exceeds the sum of the first and second terms, its value becomes negative, leading to the possibility of quadrature squeezing in F_2 .

To provide a clearer analysis of quadrature squeezing, we rely on numerical calculations, with the results presented in Figs. 2 and 3. In Fig. 2, we plot $Q_{1,\Psi}$ as a function of the parameter γ for various coupling strength parameters Γ , while the weak value $\langle\sigma_x\rangle_w = 5.671$ is fixed, corresponding to $\alpha = 8\pi/9$. As shown in Fig. 2, $Q_{1,\phi}$ ($\Gamma = 0$) remains positive and increases with γ [see the thick green curve]. Additionally, Fig. 2 demonstrates that $Q_{1,\Psi}$ for cases where $\Gamma \neq 0$ also consistently takes positive values. This observation confirms that after the postselected von Neumann measurement, the F_1 quadrature of the final MD state $|\Psi\rangle$ still doesn't exhibit squeezing, consistent with the behavior of the initial state.

In Fig. 3, we present the numerical results for $Q_{2,\Psi}$, which corresponds to the quadrature F_2 of the final MD state $|\Psi\rangle$. In Fig. 3(a), $Q_{2,\Psi}$ is plotted as a function of the state parameter γ for various coupling strength parameters Γ , with a fixed large weak value $\langle\sigma_x\rangle_w = 5.671$, corresponding to $\alpha = 8\pi/9$. Among these curves, the case $\Gamma = 0$ (thick green curve) represents $Q_{2,\phi}$ for the initial state. As shown, $Q_{2,\phi}$ decreases with increasing γ and converges to -0.125 across most parameter regions. Experimentally, the amount of squeezing is quantified in terms of decibels (dB) [64]. This value of -0.125 corresponds to 9 dB or 50% squeezing. Notably, in the specific case where the PND is $\delta = 0$, $Q_{2,\phi}$ is consistently less than zero. Thus, the initial PCS $|\phi\rangle$ with $\delta = 0$ always exhibits squeezing along the F_2 quadrature.

In Fig. 3(a), after the postselected von Neumann measurements ($\Gamma \neq 0$), we observe that the value of $Q_{2,\Psi}$ is lower than $Q_{1,\phi}$ for the weak coupling strength parameter $\Gamma = 0.3$. This behavior persists over a larger range of the state parameter γ , indicating that the squeezing characteristics of the quadrature F_2 are enhanced under postselected von Neumann measurements. However, as the coupling strength parameter Γ increases, the value of $Q_{2,\Psi}$ decreases further compared to the $\Gamma = 0.3$ case. For $\Gamma = 0.3$, the minimum value of $Q_{2,\Psi}$ reaches approximately -0.172 near $\gamma = 10$. This corresponds to a squeezing level of 11dB or 69%. Therefore, after performing postselected WMs, the quadrature squeezing along

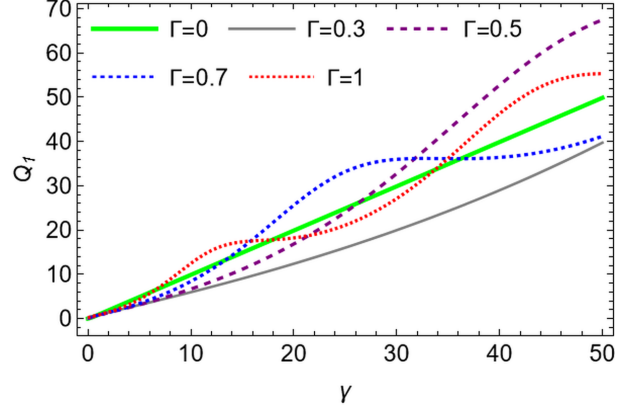


Figure 2. Quadrature squeezing $Q_{1,\Psi}$ as a function of the state parameter γ . The thick green line corresponds to the coupling strength parameter $\Gamma = 0$, representing the case where the state is the initial PCS $|\phi\rangle$. The solid gray line represents $\Gamma = 0.3$, while the purple, blue, and red dashed lines correspond to $\Gamma = 0.5$, $\Gamma = 0.7$, and $\Gamma = 1$, respectively. For these calculations, we take $\delta = 0$, $\alpha = \frac{8\pi}{9}$ and $\vartheta = 0$.

the F_2 direction of the field increases by approximately 19% under suitable system parameters and weak values of the measured system observable. To further investigate the signal amplification effect of weak values for weak system signals, Fig. 3(b) presents $Q_{2,\Psi}$ as a function of the weak value angle α for different coupling strength parameters Γ and a fixed $\gamma = 10$. The numerical results in Fig. 3(b) indicate that the weak value amplifies the squeezing effects of $Q_{2,\Psi}$ when the coupling strength parameter Γ is small, highlighting the signal amplification capability of weak measurements. These results demonstrate that the squeezing effects of $Q_{2,\Psi}$ can be enhanced by postselected WMs.

B. Sum squeezing

The sum squeezing (SQ), a higher-order of squeezing, can also characterize the nonclassicality of a two-mode radiation field. The concept of two-mode SQ for a radiation field was introduced by Hillery [65]. The sum squeezing operator is defined as:

$$V_{\varpi} = \frac{1}{2} (e^{i\varpi} a^\dagger b^\dagger + e^{-i\varpi} a b), \quad (24)$$

where the angle $\varpi \in [0, 2\pi]$. Similar to single-mode squeezing, the SQ degree $S_{ab}(\varpi)$ of a two-mode radiation field is defined as

$$S_{ab}(\varpi) = \frac{4\langle(\Delta V_{\varpi})^2\rangle}{\langle N_a + N_b + 1 \rangle} - 1, \quad (25)$$

where $\Delta V_{\varpi}^2 = \langle V_{\varpi}^2 \rangle - \langle V_{\varpi} \rangle^2$, and particle number operators for the a mode and b mode are $N_a = a^\dagger a$ and $N_b = b^\dagger b$, respectively. If $-1 \leq S_{ab}(\varpi) < 0$, the

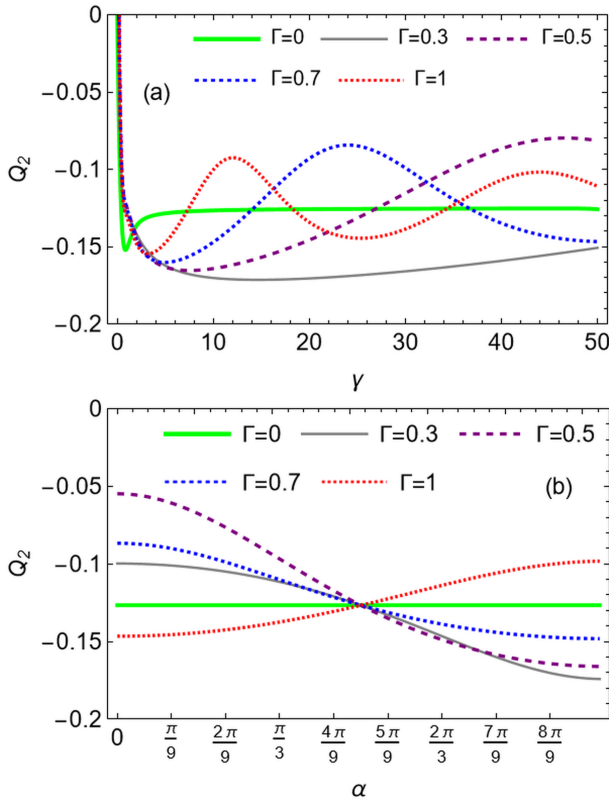


Figure 3. Quadrature squeezing $Q_{2,\Psi}$: (a) $Q_{2,\Psi}$ as a function of the state parameter γ for different coupling strength parameters Γ , with the weak value fixed at $\langle \sigma_x \rangle_w = 5.671$ corresponding to $\alpha = 8\pi/9$. (b) $Q_{2,\Psi}$ as a function of the weak value parameter α for different coupling strength parameters Γ , with the state parameter γ fixed at 10. Other parameters are the same as those in Fig. 2.

two-mode state exhibits squeezing properties. The more negative the value of $S_{ab}(\varpi)$, the greater the degree of sum squeezing in the state. The state is maximally squeezed when $S_{ab}(\varpi) = -1$. By substituting V_ϖ into Eq. (25), we obtain the squeezing degree $S_{ab}(\varpi)$ of normal-ordering operators:

$$S_{ab}(\varpi) = \frac{2 \left[\text{Re}[e^{-2i\varpi} \langle a^2 b^2 \rangle] - 2 (\text{Re}[e^{-i\varpi} \langle ab \rangle])^2 + \langle N_a N_b \rangle \right]}{\langle N_a \rangle + \langle N_b \rangle + 1} \quad (26)$$

The explicit expression of the SQ degree $S_{ab,\Psi}(\varpi)$ for the final MD state $|\Psi\rangle$ can be derived by substituting the relevant expectation values, as listed in Appendix A. When $\Gamma = 0$, no measurements are performed, and the state remains as the initial PCS $|\phi\rangle$. For this trivial case, it is straightforward to verify that the sum squeezing equals to zero, i.e., $S_{ab,\phi}(\varpi) = 0$. This result implies that, regardless of the PND δ of the two-modes or the angle ϖ , the SQ of the initial PCS $|\phi\rangle$ is always zero.

In Fig. 4, we present the SQ degree $S_{ab,\Psi}(\varpi)$ for the final MD state $|\Psi\rangle$. In Fig. 4(a), we show $S_{ab,\Psi}(\varpi)$ as a function of the state parameter γ for different val-

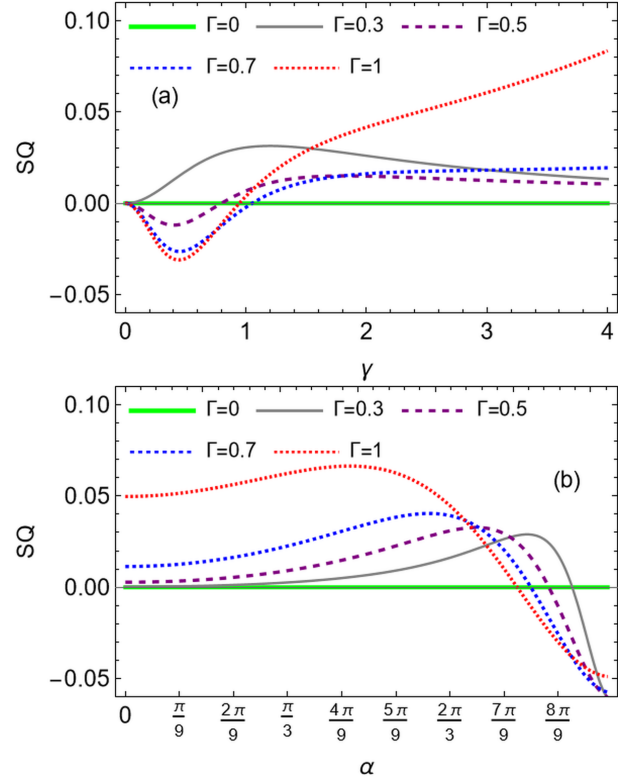


Figure 4. The SQ of the final MD state $|\Psi\rangle$ under postselected von Neumann measurement. (a) $S_{ab,\Psi}(\varpi)$ as a function of the state parameter γ for different coupling strength parameters Γ , while the weak value is fixed to $\langle \sigma_x \rangle_w = 5.671$. (b) $S_{ab,\Psi}(\varpi)$ as a function of the weak value parameter α for different coupling strength parameters Γ , while the state parameter γ is fixed at 0.5. Here, we take $\varpi = 0$. Other parameters are the same as in Fig. 2.

ues of the coupling strength parameter Γ , while fixing the weak value to $\langle \sigma_x \rangle_w = 5.671$, which corresponds to $\alpha = 8\pi/9$. As shown in Fig. 4(a), SQ occurs in a small range of the state parameter γ for appropriate coupling strengths Γ , provided the weak value of the measured system observable is large. For the anomalous weak value $\langle \sigma_x \rangle_w = 5.671$, that corresponds to $\alpha = 8\pi/9$, the minimum value of SQ degree $S_{ab,\Psi}(\varpi)$ occurs near $\gamma = 0.5$ at larger coupling strength parameters Γ . This squeezing effect diminishes as γ increases beyond this range. To further investigate the dependence of SQ on the weak value, Fig. 4(b) presents the variation $S_{ab,\Psi}(\varpi)$ as a function of the weak value parameter α for different values of Γ , while keeping $\gamma = 0.5$ fixed. As indicated in Fig. 4(b), the SQ degree $S_{ab,\Psi}(\varpi)$ takes negative values only for anomalous weak values and non-zero coupling strength parameters Γ . Notably, when the weak value angle α approaches π , the SQ effect becomes more pronounced for suitable coupling strength parameters Γ . This numerical result further confirms the amplification effect of weak values in postselected WMs within our scheme.

In the above discussions, we can conclude that the

postselected von Neumann measurement improves various squeezing characteristics of our initial PCS $|\phi\rangle$. That is to say, after postselected von Neumann measurement, the squeezing effects of $|\phi\rangle$ are enhanced for large anomalous weak values of the measured observable, with proper composite state parameters γ and coupling strength parameters Γ . Besides the squeezing effect, quantum correlation functions and entanglement, which exist between the two modes, also characterize the nature of the PCS $|\phi\rangle$. In the next sections, we investigate the effects of the postselected von Neumann measurement on the quantum correlation functions and entanglement features of the PCS $|\phi\rangle$.

IV. THE EFFECTS ON QUANTUM CORRELATION FUNCTIONS

To examine the effects of postselected von-Neumann measurement on the SOCC function $g_{ab}^{(2)}$ of the PCS, in this section, we investigate the correlation functions between the two modes.

A. Second-order cross-correlation function

The normalized SOCC of the two-mode field is defined as [66]

$$g_{ab}^{(2)} = \frac{\langle a^\dagger a b^\dagger b \rangle}{\langle a^\dagger a \rangle \langle b^\dagger b \rangle}. \quad (27)$$

Here, $\langle a^\dagger a b^\dagger b \rangle$ represents the intensity-intensity correlation between the two-modes, and $\langle a^\dagger a \rangle$ and $\langle b^\dagger b \rangle$ denote mean photon number for each mode, respectively. This function characterize the correlation between photons in the different modes. If $g_{a,b,\Psi}^{(2)} > 1$, there is correlation between the a -mode and b -mode of the two-mode radiation field. Otherwise, they are inversely correlated. To discuss the properties of $g_{a,b,\Psi}^{(2)}$, we first derive the average values of $\langle a^\dagger a b^\dagger b \rangle$, $\langle a^\dagger a \rangle$, and $\langle b^\dagger b \rangle$ under the state $|\Psi\rangle$. Since their explicit expressions are cumbersome, we list them in Appendix A. In particular, when $\Gamma = 0$, the SOCC $g_{ab,\Psi}^{(2)}$ reduces to $g_{ab,\phi}^{(2)}$ for the initial PCS $|\phi\rangle$, and its expression can be written as

$$g_{ab,\phi}^{(2)} = \frac{I_\delta(2|\gamma|)^2}{I_{\delta-1}(2|\gamma|)I_{\delta+1}(2|\gamma|)}. \quad (28)$$

As investigated in previous studies [20, 44], the cross-correlation function $g_{ab,\phi}^{(2)}$ between the a -mode and the b -mode of the PCS $|\phi\rangle$ decreases as the PND δ and the state parameter γ increase, and eventually, $g_{ab,\phi}^{(2)}$ tends to a value of 1, indicating that the correlation between the two modes is almost non-existent.

In Fig. 5 shows the variation of $g_{ab,\Psi}^{(2)}$ for different system parameters. Specifically, in Fig. 5, we plot $g_{a,b,\Psi}^{(2)}$

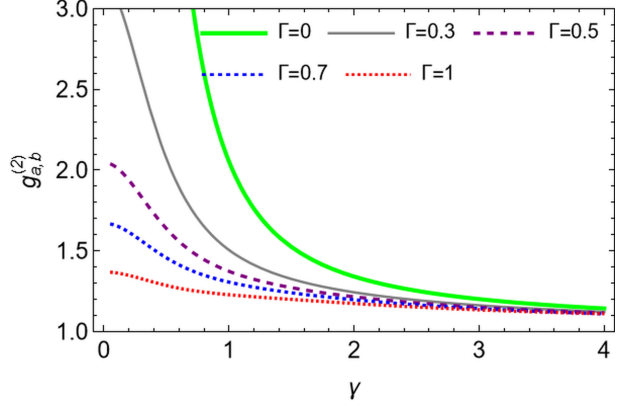


Figure 5. SOCC $g_{ab,\Psi}^{(2)}(0)$ as a function of the state parameter γ for different coupling strength parameters Γ . The green thick curve corresponds to the initial $|\phi\rangle$ case ($\Gamma = 0$). Here, we take weak value as $\langle \sigma_x \rangle_w = 5.761$ and the other parameters are the same as in Fig. 2.

as a function of the parameter γ for different coupling strength parameters Γ , while fixing the weak value to $\langle \sigma_x \rangle_w = 5.761$. As shown in Fig. 5, the SOCC $g_{ab,\Psi}^{(2)}$ of the state $|\Psi\rangle$ decreases as the coupling strength parameter Γ increases. When the state parameter γ is small, the value of $g_{ab,\Psi}^{(2)}(0)$ is greater than one. However, as γ increases, all curves tend to one. The higher the coupling strength parameters Γ , the lower the correlation between the two modes of the final MD state $|\Psi\rangle$.

B. second-order correlation function

We can examine the statistical properties of the radiation field by using the zero-time delay second-order correlation function $g^{(2)}(0)$. This function measures the intensity correlation and serves as a crucial parameter for characterizing the photon statistics of a source. For a coherent source, $g^{(2)}(0) = 1$, and for a single-photon state $g^{(2)}(0) = 0$ [67]. If $0 \leq g^{(2)}(0) < 1$, the field exhibits sub-Poissonian statistics, characterizing the non-classical features of the associated radiation field [64]. For our state $|\Psi\rangle$, the function $g^{(2)}(0)$ for each mode can be written as:

$$g_a^{(2)} = \frac{\langle a^{\dagger 2} a^2 \rangle}{\langle a^\dagger a \rangle}, \quad (29)$$

$$g_b^{(2)} = \frac{\langle b^{\dagger 2} b^2 \rangle}{\langle b^\dagger b \rangle}. \quad (30)$$

We derived the explicit expressions of $g^{(2)}(0)$ by calculating the average values of the associated operators (see Appendix A). Figure 6 displays the variations of $g_{a,\Psi}^{(2)}(0)$ and $g_{b,\Psi}^{(2)}(0)$ with the state parameter γ for different coupling strength parameters Γ . We fixed the weak value parameter at $\alpha = 8\pi/9$ to analyze the effects of large

anomalous weak values on the statistical properties of the final MD state $|\Psi\rangle$. As shown in Fig. 6, the $\Gamma = 0$ case corresponds to the $g^{(2)}(0)$ of the initial PCS state $|\phi\rangle$. Its value for both a and b -modes is smaller than one and approaches one as the state parameter γ increases (see green curves in Figs. 6(a) and 6(b)). After the postselected von Neumann measurement ($\Gamma \neq 0$), for small parameter γ , the values of the second-order correlation functions $g_a^{(2)}(0)$ and $g_b^{(2)}(0)$ quickly reach their minimum values with increasing coupling strength parameter Γ , similar to the single-photon state case. On the other hand, for large values of the state parameter ($\gamma \gg 1$), $g_a^{(2)}(0)$ and $g_b^{(2)}(0)$ become indistinguishable for all coupling strength parameters Γ and tend to one, which corresponds to the coherent state case. This result also explains why the SOCC $g_{ab,\Psi}^{(2)}$ of $|\Psi\rangle$ approaches one when $\gamma \gg 1$ (see Fig. 5).

It is interesting to note that when comparing the green thick curve ($\Gamma = 0$) with other curves in Figs. 6(a) and 6(b), the second-order correlation function of the a -mode and b -mode changes more dramatically after the postselected measurement ($\Gamma \neq 0$). Due to the weak value amplification effects, this result allows us to achieve the characteristics of a single-photon state in small regions of the state parameter γ . Our numerical results suggest that following the postselected von Neumann measurement, the two modes of the final MD state $|\Psi\rangle$ could potentially generate a single-photon field [68, 69].

V. THE EFFECTS ON ENTANGLEMENT

In this section, we investigate the effects of postselected von Neumann measurement on quantum correlations of the PCS. In a previous study [70], the inseparability of the PCS were confirmed in light of the Peres-Horodecki criterion and various entropies. Here, we separately examine the HZ correlation and EPR correlation to analyze the inseparability of the final MD state $|\Psi\rangle$, as defined in Eq. (10).

A. HZ correlation

First, we study the entanglement between the two modes in the light field by adopting the inequality provided by Hillery and Zubairy [71]. This is defined as [7]:

$$E = \langle N_a \rangle \langle N_b \rangle - |\langle ab \rangle|^2. \quad (31)$$

If $E < 0$, it implies that the state exhibits entanglement between the two modes. From the CSI, $|\langle ab \rangle|^2 \leq \langle a^\dagger a \rangle \langle b b^\dagger \rangle$ [72], the entanglement condition for two-mode fields characterized by HZ correlation is bounded as $-\langle N_a \rangle \leq E < 0$. It is straightforward to verify that the HZ correlation function E for the initial PCS $|\phi\rangle$ can

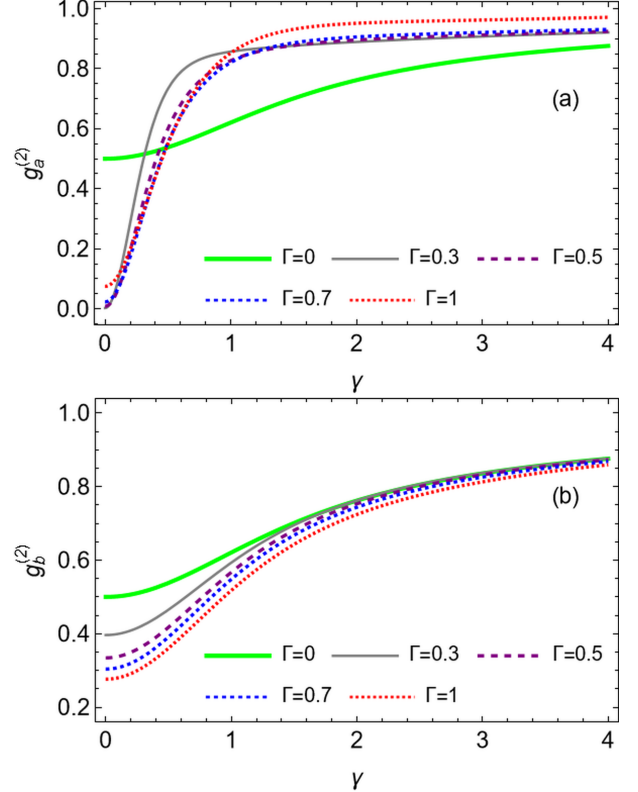


Figure 6. Second-order correlation as a function of the a and b modes of the final MD state $|\Psi\rangle$. (a) $g_{a,\Psi}^{(2)}(0)$ as a function of the state parameter γ for different coupling strength parameters Γ for mode a . (b) the b mode's $g_{b,\Psi}^{(2)}(0)$ as a function of the state parameter γ for different coupling strength parameters Γ . Here, we take weak value as $\langle \sigma_x \rangle_w = 5.761$ and other parameters are the same as in Fig. 2.

expressed as:

$$\begin{aligned} E_\phi &= \frac{|\gamma|^2 I_{\delta-1}(2|\gamma|) I_{\delta+1}(2|\gamma|)}{I_\delta(2|\gamma|)^2} - |\gamma|^2 \\ &= |\gamma|^2 \left(\frac{1}{g_{ab,\phi}^{(2)}} - 1 \right), \end{aligned} \quad (32)$$

where $g_{ab,\phi}^{(2)}$ is the SOCC defined in Eq. 28. To evaluate the HZ correlation for our output state $|\Psi\rangle$, we compute E_Ψ using Eq. (31), substituting the average values of $\langle ab \rangle$, $\langle a^\dagger a \rangle$ and $\langle b^\dagger b \rangle$ as listed in Appendix A. To demonstrate the effects of postselected von Neumann measurement on the entanglement of the output state $|\Psi\rangle$, we introduce the difference between E_Ψ and E_ϕ , defined as $\Delta E = E_\Psi - E_\phi$. Fig. 7 presents the numerical results for ΔE . If $\Delta E < 0$, it indicates that the degree of entanglement has increased compared to the initial state; otherwise, it has decreased. In Fig. 7(a), ΔE is plotted as a function of the state parameter γ for different values of PND denoted by δ , with the coupling strength parameter Γ fixed in the WM regime ($\Gamma = 0.3$) and a large anomalous weak value $\langle \sigma_x \rangle_w = 5.761$. The results

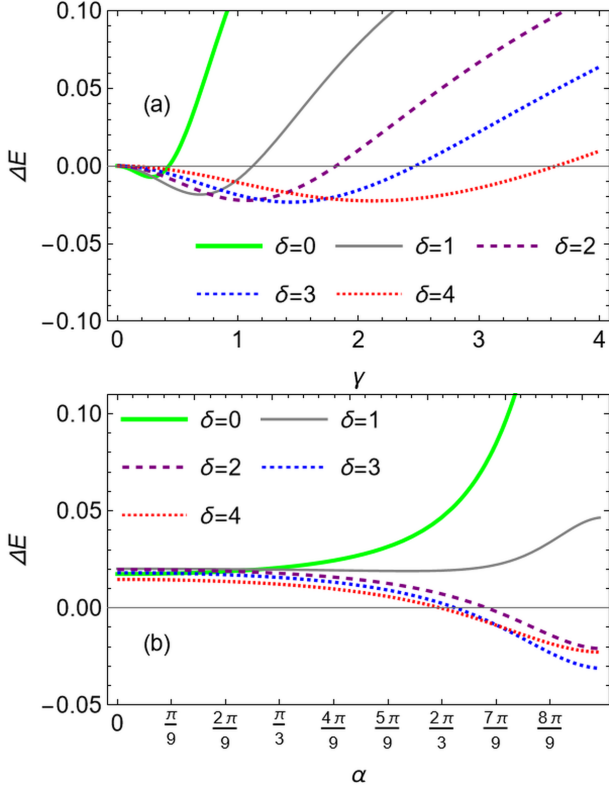


Figure 7. HZ correlation between two modes of the final MD state $|\Psi\rangle$. (a) ΔE as a function of the state parameter γ for different PND values δ , with $\langle\sigma_x\rangle_w = 5.761$. (b) ΔE as a function of the weak value parameter α for different PND values δ , with $\gamma = 1.5$. Here, we take $\Gamma = 0.3$ and other parameters are the same as in Fig. 2.

show that ΔE takes negative values for certain regions of γ , and these regions expand as δ increases. This result indicates that the final MD state $|\Psi\rangle$ exhibits stronger entangled properties than the initial PCS $|\phi\rangle$ in appropriate parameter regions. To further validate the role of weak value amplification for enhancing the entanglement between two modes of PCS after postselected measurement, Fig. 7(b) illustrates the variation of ΔE with the weak value parameter α for different values of δ . The curves in Fig. 7(b) reveal that, within the WM regime, if the PND δ between modes a and b of the PCS is equal to or greater than two (i.e., $\delta \geq 2$), the entanglement between the two modes of the measurement output state $|\Psi\rangle$ surpasses that of the initial state $|\phi\rangle$ for large anomalous weak values.

B. EPRs correlation

Another inseparability criterion for two-mode systems in multimode continuous variable systems relies on the total variance of a pair of EPR-type operators [73]. This criterion provides a sufficient condition for entanglement in any two-party continuous variable state and is also a

necessary and sufficient condition for inseparability. For a two-mode system, the EPR correlation is defined in terms of the variances of the EPR-type operators $X_1 - X_2$ and $P_1 - P_2$ as [74]

$$\begin{aligned} I &= \langle \Delta^2 (X_1 - X_2) \rangle + \langle \Delta^2 (P_1 - P_2) \rangle \\ &= 2(1 + \langle a^\dagger a \rangle + \langle b^\dagger b \rangle - \langle a^\dagger b^\dagger \rangle - \langle a b \rangle) \\ &- 2(\langle a \rangle - \langle b^\dagger \rangle)(\langle a^\dagger \rangle - \langle b \rangle). \end{aligned} \quad (33)$$

where $X_1 = \frac{a+a^\dagger}{\sqrt{2}}$, $X_2 = \frac{b+b^\dagger}{\sqrt{2}}$, $P_1 = \frac{a-a^\dagger}{i\sqrt{2}}$ and $P_2 = \frac{b-b^\dagger}{i\sqrt{2}}$. If the total variance is less than 2, $I < 2$, the two-mode system can be considered inseparable, indicating quantum entanglement. Otherwise, the system is classical. The smaller the value of I , the stronger the EPR correlation.

The explicit expression of the EPR correlation I_Ψ of our postselected measurement output state $|\Psi\rangle$ can obtained by substituting the associated averages listed in Appendix A into Eq. (33). As as special case, when $\Gamma = 0$, I_Ψ reduces to the EPR correlation I_ϕ of the initial PCS $|\phi\rangle$, and its expression reads as

$$\begin{aligned} I_\phi &= 2 \left(\frac{|\gamma| I_{\delta-1}(2|\gamma|)}{I_\delta(2|\gamma|)} + \frac{|\gamma| I_{\delta+1}(2|\gamma|)}{I_\delta(2|\gamma|)} - 2\Re(\gamma) + 1 \right) \\ &= 8Q_{2,\phi} + 2 = 8\Delta F_{2,\phi}^2. \end{aligned} \quad (34)$$

Here, $Q_{2,\phi}$ is the quadrature squeezing parameter of the initial PCS $|\phi\rangle$ as defined in Eq. (23), and $\Delta F_{2,\phi}^2$ represents the variance of the quadrature operator F_2 , defined in Eq. (17), over the state $|\phi\rangle$. For the PCS state $|\phi\rangle$, its EPR correlation is proportional to the variance $\Delta F_{2,\phi}^2$. To analyze the effects of the postselected von Neumann measurement on the EPR correlation between the two modes of the state $|\Psi\rangle$, we introduce the difference between I_Ψ and I_ϕ , defined as $\Delta I = I_\Psi - I_\phi$. To observe these effects, we plotted ΔI as a function of various system parameters, with the numerical results shown in Fig. 8. The variation of ΔI with changes in the state parameter γ for different PND δ is presented in Fig. 8(a). When the weak value is set to $\langle\sigma_x\rangle_w = 5.761$ and the coupling strength parameter is fixed at $\Gamma = 0.3$, ΔI takes negative values in a range of the state parameter γ for cases where $\delta \geq 2$. The regions of negative values become broader and deeper as the PND δ between the two modes increases. This result implies that in the postselected WM regime ($\Gamma < 1$) with large anomalous weak values, the EPR correlation between the two modes of the final MD state $|\Psi\rangle$ is stronger than that of the initial PCS state $|\phi\rangle$ when $\delta \geq 2$. Similar to the HZ correlation case, we examined the dependence of the enhancement of the entanglement on the anomalous weak values. Fig. 8(b) shows ΔI as a function of the angle α . The curves in Fig. 8(b) show that larger PND δ does not enhance the violation of the EPR correlation for small weak value angles α . However, for larger weak value angles α , ΔI becomes negative, and its absolute value increases with increasing PND δ .

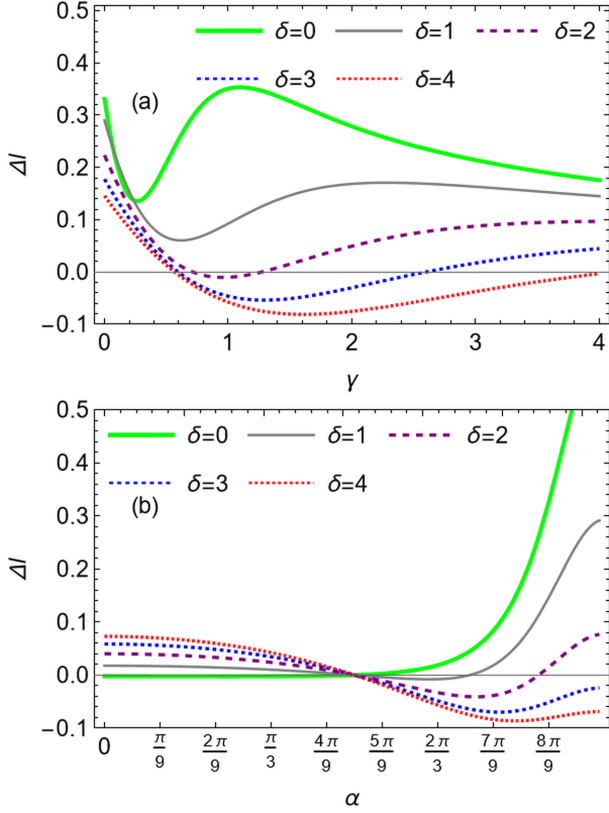


Figure 8. EPR correlation differences ΔI for the final MD state $|\Psi\rangle$ and initial PCS $|\phi\rangle$. (a) ΔI as a function of the state parameter γ for different PND δ between the two modes of the state $|\phi\rangle$. (b) ΔI as a function of the weak value angle α for different PND δ between the two modes of the state $|\phi\rangle$. Here $\Gamma = 0.3$, with (a) $\langle\sigma_x\rangle_w = 5.761$, and (b) $\gamma = 1.5$. Other parameters are the same as in Fig. 2.

In summary, the large anomalous weak values $\langle\sigma_x\rangle_w$ of the measured system observable contribute significantly to the weak signal amplification observed in our scheme.

VI. JOINT WIGNER FUNCTION

To gain a deeper understanding of the effects of post-selected von Neumann measurements on the properties of $|\Psi\rangle$, we examine the phase space distribution by calculating its Wigner function. The Wigner function of a single-mode radiation field can be written as [64]:

$$W(\alpha) = \frac{2}{\pi} \text{Tr} [\rho D(\alpha) P D^\dagger(\alpha)], \quad (35)$$

where ρ is the density operator of the given state, and $P = e^{i\pi a^\dagger a}$ is the parity operator. However, in our current work, this Wigner function cannot be used directly since the PCS is a two-mode radiation field. In the two-mode case, the Wigner function of the final MD state $|\Psi\rangle$

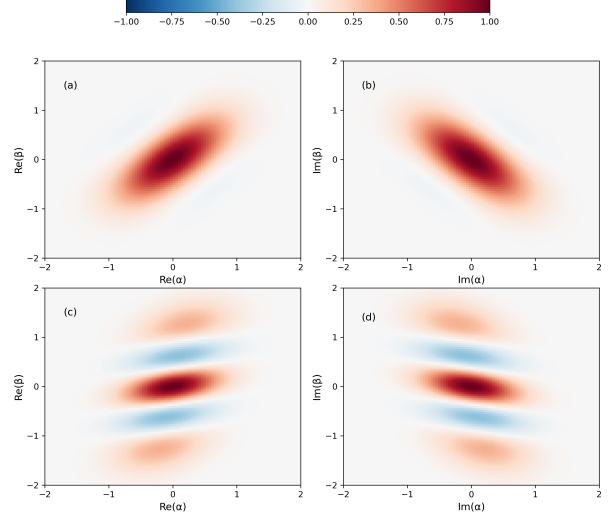


Figure 9. Cuts in the scaled two-mode Wigner function. (a and b) A 2D plane cut along (a) the $\text{Re}(\alpha) - \text{Re}(\beta)$ axes and (b) $\text{Im}(\alpha) - \text{Im}(\beta)$ axes of the calculated 4D scaled joint Wigner function $P_J(\alpha, \beta)$ for the initial PCS state $|\phi\rangle$ with $\delta = 0$. (c and d) A 2D plane cut along (c) the $\text{Re}(\alpha) - \text{Re}(\beta)$ axes and (d) the $\text{Im}(\alpha) - \text{Im}(\beta)$ axes of the calculated 4D scaled joint Wigner function $P_J(\alpha, \beta)$ of the initial PCS state $|\phi\rangle$ with $\delta = 2$. Here, $\gamma = 0.5$.

can be expressed in terms of the joint Wigner function

$$\begin{aligned} W_J(\alpha, \beta) &= \frac{4}{\pi^2} \text{Tr} [\rho D(\alpha) D(\beta) P_j D^\dagger(\beta) D^\dagger(\alpha)] \\ &= \frac{4}{\pi^2} P_J(\alpha, \beta), \end{aligned} \quad (36)$$

where $\rho = |\Psi\rangle\langle\Psi|$ is the density operator of the state $|\Psi\rangle$, $P_j = P_a P_b = e^{i\pi a^\dagger a} e^{i\pi b^\dagger b}$ is the joint photon number parity operator, and $D(\alpha) = e^{\alpha a^\dagger - \alpha^* a}$ and $D(\beta) = e^{\beta b^\dagger - \beta^* b}$ are the displacement operators acting on the a and b modes of the two-mode state $|\Psi\rangle$, respectively. The joint Wigner function W_J is a function in the 4D phase space, whose coordinates are $(\text{Re}[\alpha], \text{Im}[\alpha], \text{Re}[\beta], \text{Im}[\beta])$. In Eq. (36), $P_J(\alpha, \beta)$ is referred to as the scaled Wigner function, which we use for our analysis of the phase space distribution of the measurement output state $|\Psi\rangle$. Upon examining the expression for $P_J(\alpha, \beta)$, we find that it is the average value of the joint parity operator P_j after applying displacement operators with amplitudes $-\alpha$ and $-\beta$ to the a and b modes, respectively. Since the eigenstates of the parity operators P_a and P_b are the Fock states $|n\rangle_a$ and $|n\rangle_b$, with eigenvalues $(-1)^{n_a}$ and $(-1)^{n_b}$, the scaled Wigner function is therefore bounded by ± 1 , i.e.,

$$-1 \leq P_J(\alpha, \beta) \leq 1. \quad (37)$$

To illustrate the core features in this 4D Wigner function of the final MD state $|\Psi\rangle$ and compare it with the

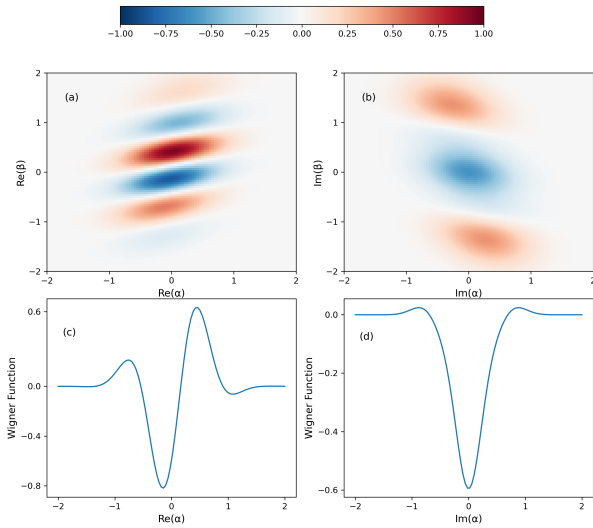


Figure 10. Joint Wigner function of the final MD state $|\Psi\rangle$ after postselected measurement. (a and b) A 2D plane cut along (a) the $Re[\alpha] - Re[\beta]$ axes and (b) the $Im[\alpha] - Im[\beta]$ axes of the calculated 4D scaled joint Wigner function $P_J(\alpha, \beta)$ for the measurement output state $|\Psi\rangle$ with $\Gamma = 0.3$, $\gamma = 0.5$, $\langle\sigma_x\rangle_w = 5.761$ and $\delta = 2$. (c) Diagonal line cuts of the data shown in (a), corresponding to a 1D plot of the calculated scaled joint Wigner function $P_J(\alpha, \beta)$ along $Re[\alpha] = Re[\beta]$ with $Im[\alpha] = Im[\beta] = 0$. (d) Diagonal line cuts of the data shown in (b), corresponding to a 1D plot of the calculated scaled joint Wigner function $P_J(\alpha, \beta)$ along $Im[\alpha] = Im[\beta]$ with $Re[\alpha] = Re[\beta] = 0$.

initial PCS state $|\phi\rangle$, we first present the 2D cuts along the $Re[\alpha] - Re[\beta]$ plane and the $Im[\alpha] - Im[\beta]$ plane of the joint Wigner function of $|\phi\rangle$, as shown in Fig. 9. Figs. 9(a) and 9(b) represent the density plot of the joint Wigner function of the initial PCS state $|\phi\rangle$ with $\gamma = 0.5$ and $\delta = 0$, in the planes $Im[\alpha] = Im[\beta] = 0$ and $Re[\alpha] = Re[\beta] = 0$, respectively. As shown in these figures, the initial PCS $|\phi\rangle$ is Gaussian when there is no PND between the two modes ($\delta = 0$), and it exhibits squeezing along the F_2 quadrature [see Sec. III A]. Similarly, Figs. 9(c) and 9(d) show the density plots of the joint Wigner function of the initial PCS state $|\phi\rangle$ with $\gamma = 0.5$ and $\delta = 2$, in the planes $Im[\alpha] = Im[\beta] = 0$ and $Re[\alpha] = Re[\beta] = 0$, respectively. It is evident that when there is PND between the two modes ($\delta = 2$), the state $|\phi\rangle$ becomes non-Gaussian. Additionally, the characteristic interference fringes of the PCS are visible, indicating substantial coherence and consistent multiphoton phases. This result suggests that PND ($\delta \neq 0$) between the two modes is crucial for enhancing the nonclassicality of the PCS state $|\phi\rangle$.

In Fig. 10, we present the scaled joint Wigner function $P_J(\alpha, \beta)$ of the final MD state $|\Psi\rangle$ with $\Gamma = 0.3$, $\gamma = 0.5$, $\langle\sigma_x\rangle_w = 5.761$, and $\delta = 2$. We observe that

this Wigner function exhibits highly nonclassical characteristics in phase space. Compared to the initial PCS state $|\phi\rangle$ [see Figs. 9 (c) and 9 (d)], we can see that after the postselected measurement, the shapes of the scaled joint Wigner functions not only show good squeezing for the appropriate coupling strength parameter Γ and large anomalous weak value $\langle\sigma_x\rangle_w$, but we also can observe clear quantum interference structures formed between the peaks [see Figs. 10 (c) and 10 (d)]. Furthermore, if someone take comparison Fig. 9 and Fig. 10 who can find that after postselected von Neumann measurement the negative values of Wigner function increased for large anomalous weak value compared to initial state case. This indicated that the nonclassicality of the PCS enhanced after the postselected von Neumann measurement.

These phase space analyses demonstrate that after the postselected von Neumann measurement, the nonclassicality and non-Gaussianity of PCS state $|\phi\rangle$ is enhanced due to the weak signal amplification feature of the weak value.

VII. FIDELITY

To deeply understand the effects of postselected von Neumann measurement on the initial PCS, in this section we study state distance between initial and final MD state corresponding to the before and after measurement process, and the teleportation fidelity.

A. State distance

In this sub-section, we examine the state distance between the initial PCS and final MD states, specifically $|\phi\rangle$ and $|\Psi\rangle$ using the fidelity function. The fidelity F is defined as the square of the absolute value of their scalar product, and it is bounded as $0 \leq F \leq 1$, where the lower (higher) boundary represents completely different (identical) states. We define the fidelity function between $|\phi\rangle$ and $|\Psi\rangle$ as:

$$F = |\langle\phi|\Psi\rangle|^2. \quad (38)$$

After substituting $|\phi\rangle$ and $|\Psi\rangle$ (see Eqs. (1) and (10)) into the above formula, one can derive an explicit expression for F . However, we only present the numerical analysis of this quantity. As shown in Fig. 11, the postselected von Neumann measurement indeed causes a change in the given state, resulting in a larger state distance between $|\phi\rangle$ and $|\Psi\rangle$, which even transforms it into a distinguishable state with increasing coupling strength parameter Γ and state parameter γ . Larger anomalous weak values have a more significant effect than smaller ones in distinctly transforming between the states.

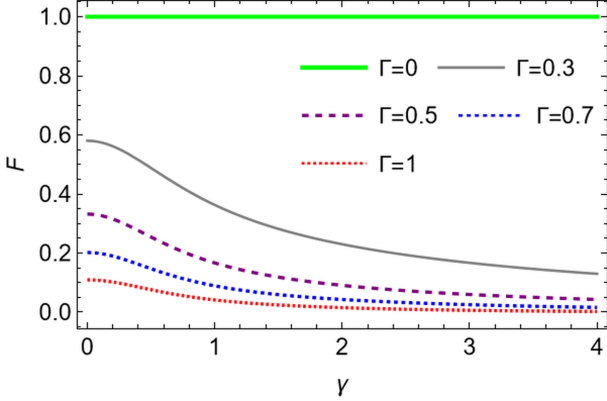


Figure 11. Fidelity F as a function of the state parameter γ . Here, we take weak value as $\langle \sigma_x \rangle_w = 5.761$ and other parameters are the same as Fig. 2.

B. Fidelity of teleportation

As discussed in Sec. V, the postselected von Neumann measurement can enhance the entanglement between two modes of PCS for some parameter regions. We know that the distillation or purification of entanglement are vital to realize the long-standing quantum communication. In order to check the effects of our von Neumann-type measurement on the efficiency of teleportation by using the PCS as the entangled channel, we use the fidelity to measure the performance of entanglement.

Here we consider the protocol of quantum teleportation was proposed by Vaidman, Braunstein and Kimble (called VBK protocol) [75–77]. We take the final MD state $|\Psi\rangle_{ab}$ [see the Eq. (10)] as the teleportation channel to teleport a coherent state by using VBK protocol. Next, we briefly describe the teleportation processes. We assume that as the sender and recipient the Alice and Bob possess and could control the a mode and b mode of the state $|\Psi\rangle_{ab}$, respectively, and the there have a coherent state $|\alpha\rangle_c$ in c mode to be teleported. Thus, initially the composite three modes state takes the form $|\Psi_1\rangle = |\Psi\rangle_{ab}|\alpha\rangle_c$. Firstly, Alice take a joint measurement of the orthogonal quadrature components of modes a and c characterized by [78]

$$|\beta\rangle_{ac} = \frac{1}{\sqrt{\pi}} \sum_{k=0}^{\infty} D_c(\beta) |k\rangle_a |k\rangle_c, \quad (39)$$

where $D_c(\beta)$ represents the displacement operator acting on mode c . After the joint measurement the state $|\Psi_1\rangle$ changes to $|\Psi_2\rangle = {}_{ac}\langle \beta |\Psi_1\rangle$. Then, Alice communicate with Bob with classical information channel and tell the information of the parameter β . Finally, Bob takes a displacement operation over his b mode according to the received value of β from Alice. After all operations are

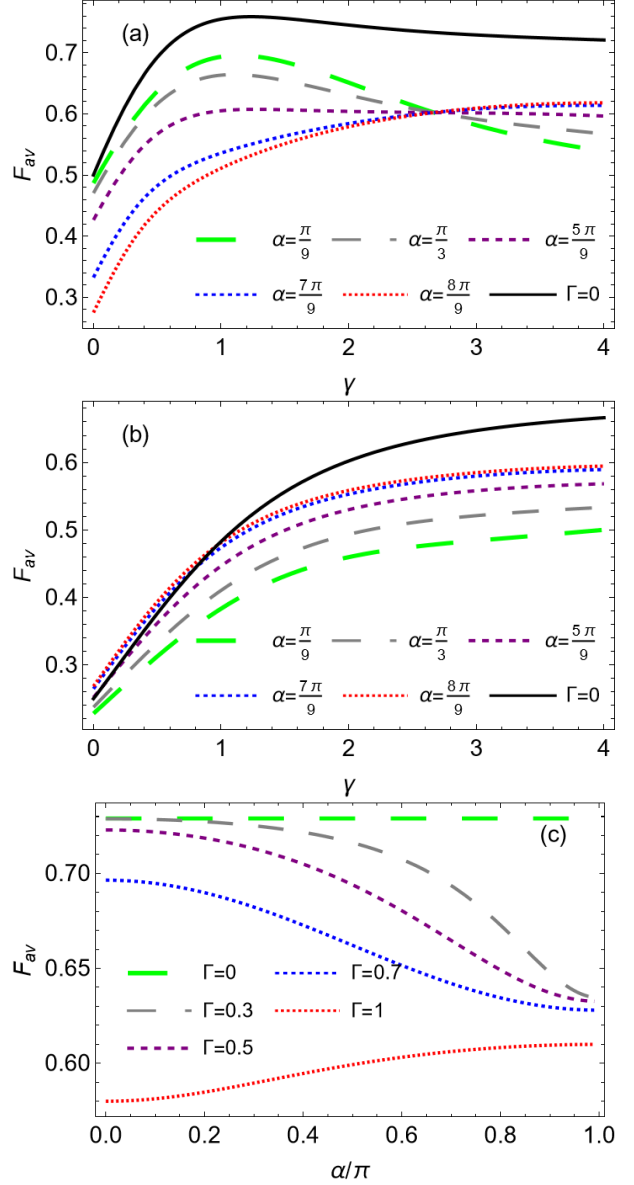


Figure 12. The fidelity of teleportation of coherent state for different system parameters. The (a) and (b) present the fidelity of teleportation as a function of PCS state parameter γ for different values of α . The (c) shows the fidelity of teleportation as a function of weak value parameter α for different coupling strength parameter Γ while fixed $\gamma = 3$ and $\delta = 0$. In (a) $\delta = 0$ and (b) $\delta = 1$, and $\Gamma = 1$ in both cases, and other parameters are the same as Fig. 2.

completed, the resulting state at Bob's side is given as

$$|\Psi_b\rangle = \frac{\mathcal{N}_\delta \lambda}{2\sqrt{\pi}} \sum_{n,m=0}^{\infty} \frac{\gamma^{n+\delta/2} h_m}{\sqrt{n!(n+\delta)!}} \times (t_+ J_{+,mn} + t_- J_{-,mn}) D_b(\beta) |n\rangle_b, \quad (40)$$

where, $h_m = \langle m | D_c(-\beta) | \alpha \rangle_c$, $t_\pm = 1 \pm \langle \sigma_x \rangle_w$ and $J_{\pm,mn} = \langle m | D_a(\pm \frac{\Gamma}{2}) | n + \delta \rangle_a$.

To evaluate this teleportation process we can rely on

the average fidelity defined by

$$F_{av} = \int d^2\beta |\langle \alpha | \Psi_b \rangle|^2. \quad (41)$$

The above integral have exact value and its explicit expression is listed in Appendix A. The teleportation process is considered successful when $0.5 < F_{av} \leq 1$ and the higher average fidelity indicates the better quality of the teleportation process. In Fig. 12 we plot the average fidelity F_{av} of the teleportation as a function of γ for different weak value parameter α . The black curves in Fig. 12 (a) and (b) corresponding to the $\delta = 0$ and $\delta = 1$ cases of initial PCS $|\phi\rangle$. It can observe that the average fidelity F_{av} significantly dependent on the PND δ . When the PND is set to $\delta = 0$, its corresponding average teleportation fidelity is fully higher than the case of $\delta = 1$ for whole parameter regimes. For $\delta = 0$ case the maximum value 0.7589 of F_{av} achieved at near $\gamma \approx 1.22$.

As showed in Fig. 12 (a), for $\delta = 0$ case in small state parameter γ regions the postselected von Neumann measurement have no positive effect on the teleportation task if the weak value $\langle \sigma_x \rangle_w$ takes anomalous values. However, with increasing the parameter γ the average fidelity F_{av} also increases along with large weak values. For $\delta = 0$ case, if $\gamma > 0.9$ the average fidelity always larger than the minimum value (i.e., 0.5) of successful teleportation and this claim is valid for all $\Gamma \leq 1$ regimes [see the Fig. 12 (c)].

In Fig. 12 (b) we presented the average fidelity F_{av} for $\delta = 1$ case. It can be seen that in small state parameter ($\gamma < 1$) regions the postselection operation could let the F_{av} take larger value than the initial PCS whereas those values can't guarantee the successful teleportation. However, in $\gamma > 1$ regions of $\delta = 1$, same as $\delta = 0$ case, after the postselected von Neumann measurement the average fidelity still can't beyond the initial PCS. One interesting point in $\delta = 1$ case is that with increase the state parameter γ and weak value the F_{av} also increasing, and can exceed 0.5 for large anomalous weak values and large γ .

In a word, compared with the initial PCS state $|\phi\rangle$ the postselected von Neumann measurement ($\Gamma \neq 0$) can't enhance the performance of successful teleportation of coherent state if we take the state $|\Psi\rangle_{ab}$ as quantum channel. But, for PND $\delta = 0$ and $\delta = 1$ cases, the postselected von Neumann measurement also could guarantee to keep the successful teleportation in weak measurement regimes with anomalous weak values.

VIII. DISCUSSION

From the fidelity analysis of our measurement output, the final MD state $|\Psi\rangle$, we can deduce that after the postselected von Neumann measurement, the initial PCS $|\phi\rangle$ undergoes a dramatic change, potentially transforming into a completely different state. As previous related studies have shown, the postselected von Neumann measurement technique provides an alternative approach to

state engineering processes and guarantee the high fidelity [41]. In most usual state preparation and state optimization methods the photon addition and /or photon subtraction are necessary [21, 22, 30–32], but if one use the postselected von Neumann measurement method to state preparation processes who can prepare the photon added or photon subtracted quantum states without adding or subtracting photons [41]. In this context, we explore the concrete changes of the final MD state $|\Psi\rangle$ in state preparation processes. Depending on the coupling strength parameter Γ and the state parameter γ , we outline its usefulness in the following four scenarios:

(1) Arbitrary values for the state parameter γ and the coupling strength parameter Γ . In this general case, our final MD state is the measurement output state $|\Psi\rangle$ as defined in Eq. (10). For simplicity, the initial PCS $|\phi\rangle$ expressed in the coherent state representation as [44].

$$|\phi\rangle = \mathcal{N}_\delta e^{|\gamma|} \int \frac{d\theta}{2\pi} \left[(\gamma)^{1/2} e^{i\theta} \right]^{-\delta} |(\gamma)^{1/2} e^{i\theta} \rangle_a |(\gamma)^{1/2} e^{-i\theta} \rangle_b. \quad (42)$$

Here, $|(\gamma)^{1/2} e^{i\theta} \rangle_a = D(\sqrt{\gamma} e^{i\theta}) |0\rangle_a$ and $|(\gamma)^{1/2} e^{-i\theta} \rangle_b = D(\sqrt{\gamma} e^{-i\theta}) |0\rangle_b$ denote the coherent states corresponding to the a and b modes of PCS. In this case, we can rewrite the $|\Psi\rangle$ as the following from

$$|\Psi\rangle = \frac{\lambda}{2} \left[t_+ |\gamma + \frac{\Gamma_a}{2}, \delta\rangle + t_- |\gamma - \frac{\Gamma_a}{2}, \delta\rangle \right]. \quad (43)$$

Here, the state $|\gamma \pm \frac{\Gamma_a}{2}, \delta\rangle$ represents the displaced PCS (the displacement operator $D(\pm \frac{\Gamma}{2})$ acts only on a mode), and its expression is given by:

$$|\gamma \pm \frac{\Gamma_a}{2}, \delta\rangle = \frac{\mathcal{N}_\delta e^{|\gamma|}}{2\pi} \int \left[(\gamma)^{1/2} e^{i\theta} \right]^{-\delta} e^{\pm \frac{\Gamma}{2} [iIm[((\gamma)^{1/2} e^{-i\theta})^*]]} \times |(\gamma)^{1/2} e^{i\theta} \pm \frac{\Gamma}{2} \rangle_a |(\gamma)^{1/2} e^{-i\theta} \rangle_b d\theta. \quad (44)$$

The final MD state $|\Psi\rangle$ is the superposition of $|\gamma + \frac{\Gamma_a}{2}, \delta\rangle$ and $|\gamma - \frac{\Gamma_a}{2}, \delta\rangle$. By taking the postselection probability of measured system (it equals to $|\langle \psi_f | \psi_i \rangle|^2$) into account, the success probability of postselection of our MD state is [79, 80]

$$P_s = \langle \phi' | \phi' \rangle = \frac{1}{2} \cos^2 \frac{\alpha}{2} [1 + |\langle \sigma_x \rangle_w|^2 + (1 - |\langle \sigma_x \rangle_w|^2) P] \quad (45)$$

where $|\phi'\rangle = \langle \psi_f | \Psi_{evol} \rangle$ and the expression of $|\Psi_{evol}\rangle$ is given in Eq. (9). For $\delta = 0$ case, the dependence of P_s on the weak value $\langle \sigma_x \rangle_w$ and coupling strength parameter Γ for fixed state parameter γ is presented in Fig. 13. As showed Fig. 13, the success probability of postselection of our MD state is not very low especially in very weak coupling and small weak values regimes. With increase the coupling strength parameter Γ the P_s is decreasing

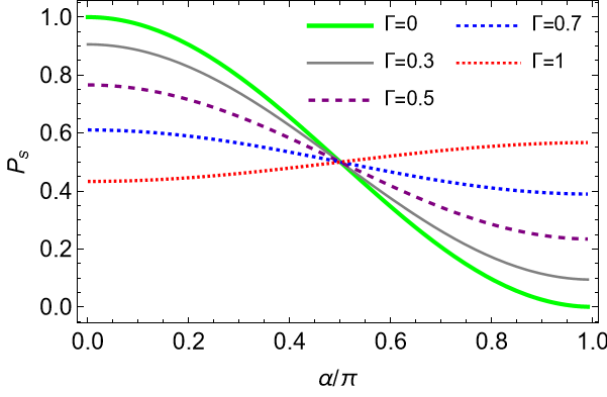


Figure 13. The success probability of postselection of the final MD state $|\Psi\rangle$ as a function weak value parameter α for different coupling strength parameter Γ . Here, we take $\delta = 0$, $\gamma = 2$ and other parameters are the same as Fig. 2.

for normal weak values of system observable. Whereas, if $\langle\sigma_x\rangle_w$ take anomalous values ($\frac{\pi}{2} < \alpha < \pi$), the output state detected probability P_s increased with increasing the coupling strength Γ .

(2) Strong coupling strength parameter ($\Gamma > 1$) with small state parameter γ ($|\gamma| \ll 1$). Since the state parameter γ is very small, we expand the Eq. (1) up to the first order of γ and ignore higher order terms. In this extreme case, the Eq. (43) changed to:

$$|\Psi'\rangle \approx \frac{\lambda'}{2} \left\{ \left[t_+ \left| \frac{\Gamma}{2}, \delta \right\rangle_a + t_- \left| -\frac{\Gamma}{2}, \delta \right\rangle_a \right] |0\rangle_b + \frac{\gamma}{\sqrt{1+\delta}} \left[t_+ \left| \frac{\Gamma}{2}, 1+\delta \right\rangle_a + t_- \left| -\frac{\Gamma}{2}, 1+\delta \right\rangle_a \right] |1\rangle_b \right\}, \quad (46)$$

where $\lambda' = \frac{\sqrt{2}\gamma^{\delta/2}}{\sqrt{\delta!}} [1 + |\langle\sigma_x\rangle_w|^2 + (1 - |\langle\sigma_x\rangle_w|^2)P]^{-\frac{1}{2}}$. The states $|\pm\frac{\Gamma}{2}, \delta\rangle_a = D(\pm\frac{\Gamma}{2})|\delta\rangle_a$ and $|\pm\frac{\Gamma}{2}, 1+\delta\rangle_a = D(\pm\frac{\Gamma}{2})|1+\delta\rangle_a$ denote the displaced δ and $1+\delta$ photon Fock states of the a -mode, respectively. It can be observed that the state $|\Psi'\rangle$ is entangled state of the a and b -modes, and interesting quantum phenomena in the a -mode can be explored by adjusting the related parameters.

If $\langle\sigma_x\rangle_w = 0$, i.e. $\alpha = 0$, the Eq. (46) changed to

$$|\Psi'_{ch}\rangle \approx \left\{ \left[\left| \frac{\Gamma}{2}, \delta \right\rangle_a + \left| -\frac{\Gamma}{2}, \delta \right\rangle_a \right] |0\rangle_b + \frac{\gamma}{\sqrt{1+\delta}} \left[\left| \frac{\Gamma}{2}, 1+\delta \right\rangle_a + \left| -\frac{\Gamma}{2}, 1+\delta \right\rangle_a \right] |1\rangle_b \right\}. \quad (47)$$

In this expression the entangled state between two modes can be seen very clearly. If the b -mode is in the vacuum state $|0\rangle_b$, and the a -mode is in superposition of displaced Fock state, i.e., $|\frac{\Gamma}{2}, \delta\rangle_a + |-\frac{\Gamma}{2}, \delta\rangle_a$. In this case, an interesting point is that if the PND between the two modes is

zero ($\delta = 0$), the a mode is prepared in even Schrödinger cat state $|\frac{\Gamma}{2}\rangle + |-\frac{\Gamma}{2}\rangle$. If we take measurement on mode b and detect a single photon, the a mode prepared in the superposition of displaced number states:

$$|\phi\rangle_a \sim \langle 1|_b (|\Psi'_{ch}\rangle) \sim \left[D\left(\frac{\Gamma}{2}\right) + D\left(-\frac{\Gamma}{2}\right) \right] |1+\delta\rangle_a, \quad (48)$$

Furthermore, if $\langle\sigma_x\rangle_w = 1$, the above state became another entangled state as

$$|\psi_{ch}\rangle = \left| \frac{\Gamma}{2}, \delta \right\rangle_a |0\rangle_b + \frac{\gamma}{\sqrt{1+\delta}} \left| \frac{\Gamma}{2}, 1+\delta \right\rangle_a |1\rangle_b. \quad (49)$$

It can be seen that if the b -mode in the vacuum state $|0\rangle_b$ then a mode stated in displaced PND state $D(\frac{\Gamma}{2})|\delta\rangle_a$. Upon detecting a single photon at mode b , mode a collapses to displaced $1+\delta$ photon state:

$$|\phi\rangle_a \sim \langle 1|_b (|\psi_{ch}\rangle) \sim D\left(\frac{\Gamma}{2}\right) |1+\delta\rangle_a. \quad (50)$$

(3) Weak coupling strength parameter ($\Gamma \ll 1$) with state parameter γ ($|\gamma| > 1$). In this case, since the coupling strength Γ is small, we can perform a first-order Taylor expansion of the associated operators; The displacement operator is approximately $D(\frac{\Gamma}{2}) \approx \mathbb{I} + \frac{\Gamma}{2}(a^\dagger - a)$. Then, the final MD state $|\Psi\rangle$ (Eq. (10)) changes to (unnormalized):

$$|\Psi''\rangle \approx \left[1 + \frac{\Gamma}{2}(a^\dagger - a) \text{Re}[\langle\sigma_x\rangle_w] \right] |\phi\rangle, \quad (51)$$

In this case, the state $|\Psi''\rangle$ is in a superposition of the PCS, single-photon-added PCS, and single photon-subtracted PCS. Most of the phenomena observed in our current work arise from this state.

(4) Weak coupling strength parameter ($\Gamma \ll 1$) with small state parameter γ ($|\gamma| < 1$). Here, as both the coupling parameter $\Gamma < 1$ and γ are very small, we can neglect $\Gamma\gamma^{1+\delta/2}$ and higher-order terms in our system state. In this extreme case, the expression for our output state $|\Psi\rangle$ further changes to (unnormalized):

$$|\Psi'''\rangle \approx \left\{ \left[|\delta\rangle_a + \frac{\Gamma}{2} \text{Re}[\langle\sigma_x\rangle_w] \sqrt{\delta+1} |\delta+1\rangle_a \right. \right. \\ \left. \left. - \frac{\Gamma}{2} \text{Re}[\langle\sigma_x\rangle_w] \sqrt{\delta} |\delta-1\rangle_a \right] |0\rangle_b \right. \\ \left. + \frac{\gamma}{\sqrt{1+\delta}} |1+\delta\rangle_a |1\rangle_b \right\}. \quad (52)$$

In this regime, the WVA is dominant, and $\Gamma\text{Re}[\langle\sigma_x\rangle_w]$ can be take big quantity compared to γ with low success probability of postselection, especially if the pre and post-selected system states are nearly orthogonal. If we assume the PND equal zero ($\delta = 0$) and , the a -mode is

prepared in a superposition state of $|0\rangle_a$ and $|1\rangle_a$, while the b -mode remains in the vacuum state:

$$|\phi'''\rangle_a \sim \langle 0|_b (|\Psi'''\rangle) \sim |0\rangle_a + \frac{\Gamma}{2} \text{Re}[\langle \sigma_x \rangle_w] |1\rangle_a. \quad (53)$$

Furthermore, under sufficiently large anomalous weak value, it is possible to detect a single photon from the a -mode. This feature could be useful in quantum computation processes, as discussed in [81]. More interestingly, in this extreme case, we can also prepare the state $|1 + \delta\rangle_a |1\rangle_b$, but with a lower success probability of post-selection. For this extreme case, the advantages of our scheme are highlighted by the very small value regimes shown in the numerical results of Figs. 6 (a) and 6 (b). As we observed, the above prepared states all strongly depends on PND δ of PCS, and we can obtain various displaced photon numbers states and their superposition states just by changing δ without photon addition or photon subtraction processes.

In recent study [31], the enhancement of non-Gaussianity and nonclassicality of PCS is investigated by adding k photons on a -mode while subtracting l photons from the b -mode, and showed that the features including squeezing, quantum correlations and phase space distributions of initial PCS are improved if k and l both greater than one (i.e. $k, l \gg 1$). Furthermore, in Ref. [82] the same task is considered via subtraction photons from two modes of PCS simultaneously and obtained similar results as in [31]. However, it's important to mention that photon addition and/or subtraction operation are probabilistic processes, generally having low success rates even for single photon addition and/or subtraction case. For example, the non-Gaussian optical states can be generated via heralding schemes using photon detectors, with typically use beam splitters to realize the photon subtraction [83]. In this case, the transmissivity parameters must be considered when modeling the photon subtraction through a beam splitter, which dramatically reduces the probability of successful state optimization. The accomplishments of above mentioned multiphoton addition and/or subtraction processes need more than one beam splitters and higher precision to photon detectors. Needless to say, such multiphoton addition and/or subtraction operation based optimization to the PCS have very low success efficiency.

Compared with previous state optimization methods, our postselected von Neumann measurement based optimization on PCS is easy to preform and doesn't need any photon addition and/or subtraction operations. In our scheme the output state detected probability is not very low [see Fig.13] and the efficiency also can be controlled by adjusting the coupling strength parameter and weak values. However, our state optimization method also has its limitations. With the existence of postselection process, we can select partial information based on our wanted outcome and discard the information from the initially prepared state. On the other hand, the large anomalous weak values are often accompanied by a low

probability of successful postselection. Due to these limitations, obtaining the desired results via this method requires a large number of repeated measurements on the prepared systems as any precision measurements accomplished with postselected weak measurement [84, 85].

We also note that our theoretical scheme could be realized on an optical platform, as the initial system preparation, post-selection of the measured system, and weak coupling between the measured system and MD can all be accomplished in optical labs, as in previous WVA experiments [86, 87]. Furthermore, it may also be possible to implement our scheme in a trapped ion system, as the von Neumann-type interaction Hamiltonian $H_{int} = g\sigma_x \otimes P_x$ can be prepared in two-dimensional harmonic oscillators of trapped ion systems [51, 88–91].

Finally, the postselected von Neumann measurement utilizes the technique of WVA, which enables the PCS to exhibit excellent non-classical properties. The PCS under postselected von Neumann measurement can show improved performance in squeezing, quantum statistics, and entanglement by selecting appropriate parameters. This method may provide a valuable quantum resource for checking and enhancing the efficiency of associated quantum tasks based on PCS [10, 55, 56].

IX. CONCLUSION

In this paper, we have proposed a theoretical model to enhance the non-Gaussianity and nonclassicality of PCS using postselected von Neumann measurement. We apply a postselected measurement to one mode (the a -mode) of the PCS and investigate related properties, including squeezing, quantum statistics, and entanglement. The results show that after the postselected von Neumann measurement, the associated characteristics of the measurement output state are enhanced in the WM regime with anomalous weak values. Quadrature squeezing achieves better-squeezing effects than the PCS over a wide range of state parameters γ under WM. The sum squeezing effect occurs due to WVA for larger weak values. Numerical results using HZ correlation and EPR correlation also show that the entanglement between the two modes of the postselected measurement-enhanced PCS becomes stronger than the initial state. We confirm these findings by examining the scaled joint Wigner function for different system parameters. We also analyze the changes in the initial state after the measurement process in terms of fidelity and observe that as the coupling strength parameter Γ increases, the initial state $|\phi\rangle$ changes and can even become orthogonal to $|\phi\rangle$. From this perspective, we also discuss the potential applications of our scheme in quantum state preparation processes and found that various quantum states with high probability could be generated with some additional measurement procedures. Interestingly, we also noticed that with our enhanced PCS the photon addition non-Gaussian states also can be generated without

actual photon addition operations.

Furthermore, as an application example of the PCS under postselected von Neumann measurement, we also explore the quantum teleportation protocol by using the postselected measurement-enhanced PCS as quantum channel. The results showed that in weak measurement regimes the successful teleportation of a coherent state via our enhanced PCS-based quantum channel for anomalous weak values could be implemented, but the corresponding averages fidelity still lower than the initial PCS case. Even though this drawback, the existence of the postselected von Neumann measurement could lead the average fidelity be higher than the minimum limit value for successful quantum teleportation, so that the teleportation of the associated quantum information with our enhanced PCS-based quantum channel is still guaranteed.

We explored the possibility of performing postselected von Neumann measurements in multimode radiation fields. For simplicity, we only considered the postselected measurement on one mode of the PCS. It would be interesting to extend this to postselected measurements on both modes of two-mode states, such as the two-mode squeezed vacuum state, to generate interesting

states, including entangled superpositions of two coherent states [4]. In future work, it will also be interesting to study the effects of postselected von Neumann measurements on other Gaussian and non-Gaussian multipartite continuous-variable radiation fields [1, 2, 92], as well as their practical applications and implementations in the laboratory.

ACKNOWLEDGMENTS

This work was supported by the National Natural Science Foundation of China (No. 12365005).

Appendix A: Related expression

Here, we derive explicit expressions for the relevant average values and teleportation fidelity F_{av} associated with our proposed state $|\Psi\rangle$. However, due to their complexity, many of these expressions are too cumbersome to include in the main text. Therefore, we have provided them in this appendix for reference.

$$\begin{aligned} \langle a^\dagger a \rangle &= \frac{|\lambda|^2}{2} \left[(1 + |\langle \sigma_x \rangle_w|^2) P_{11} + (1 - |\langle \sigma_x \rangle_w|^2) P_{12} \right], \\ P_{11} &= \frac{|\gamma| I_{\delta-1}(2|\gamma|)}{I_\delta(2|\gamma|)} + \frac{\Gamma^2}{4}, \\ P_{12} &= \mathcal{N}_\delta^2 \sum_{n=0}^{\infty} \frac{|\gamma|^{2n+\delta}}{n!(n+\delta-1)!} e^{-\frac{\Gamma^2}{2}} L_{n+\delta}^{(0)}(\Gamma^2) \\ &\quad - \frac{\Gamma}{2} \mathcal{N}_\delta^2 \sum_{n=0}^{\infty} \frac{|\gamma|^{2n+\delta}}{n!(n+\delta)!} e^{-\frac{\Gamma^2}{2}} \Gamma L_{n+\delta}^{(1)}(\Gamma^2) \\ &\quad + \frac{\Gamma}{2} \mathcal{N}_\delta^2 \sum_{n=0}^{\infty} \frac{|\gamma|^{2n+\delta}}{n!(n+\delta)!} e^{-\frac{\Gamma^2}{2}} \Gamma L_{n+\delta-1}^{(1)}(\Gamma^2) \\ &\quad + \frac{\Gamma^2}{4} \mathcal{N}_\delta^2 \sum_{n=0}^{\infty} \frac{|\gamma|^{2n+\delta}}{n!(n+\delta)!} e^{-\frac{\Gamma^2}{2}} L_{n+\delta}^{(0)}(\Gamma^2). \end{aligned} \quad (A1)$$

$$\begin{aligned} \langle b^\dagger b \rangle &= \frac{|\lambda|^2}{2} \left[(1 + |\langle \sigma_x \rangle_w|^2) P_{21} + (1 - |\langle \sigma_x \rangle_w|^2) P_{22} \right], \\ P_{21} &= \frac{|\gamma| I_{\delta+1}(2|\gamma|)}{I_\delta(2|\gamma|)}, \\ P_{22} &= \mathcal{N}_\delta^2 \sum_{n=0}^{\infty} \frac{|\gamma|^{2n+\delta}}{(n-1)!(n+\delta)!} e^{-\frac{\Gamma^2}{2}} L_{n+\delta}^{(0)}(\Gamma^2). \end{aligned} \quad (A2)$$

$$\langle ab \rangle = \frac{|\lambda|^2}{2} \left[(1 + |\langle \sigma_x \rangle_w|^2) P_{31} + (1 - |\langle \sigma_x \rangle_w|^2) P_{32} \right], \quad (\text{A3})$$

$$P_{31} = \gamma,$$

$$P_{32} = \mathcal{N}_\delta \mathcal{N}_{\delta-1} \sum_{n=0}^{\infty} \frac{(\gamma^*)^{-1} |\gamma|^{2n+\delta}}{(n-1)!(n-1+\delta)!} e^{-\frac{\Gamma^2}{2}} L_{n+\delta-1}^{(0)}(\Gamma^2)$$

$$- \frac{\Gamma^2}{2} \mathcal{N}_\delta \mathcal{N}_{\delta-1} \sum_{n=0}^{\infty} \frac{(\gamma^*)^{-1} |\gamma|^{2n+\delta}}{(n-1)!(n+\delta)!} e^{-\frac{\Gamma^2}{2}} L_{n+\delta-1}^{(1)}(\Gamma^2).$$

$$\langle a^2 b^2 \rangle = \frac{|\lambda|^2}{2} \left[(1 + |\langle \sigma_x \rangle_w|^2) P_{41} + (1 - |\langle \sigma_x \rangle_w|^2) P_{42} \right], \quad (\text{A4})$$

$$P_{41} = \gamma^2,$$

$$P_{42} = \mathcal{N}_\delta \mathcal{N}_{\delta-2} \sum_{n=0}^{\infty} \frac{(\gamma^*)^{-2} |\gamma|^{2n+\delta}}{(n-2)!(n-2+\delta)!} e^{-\frac{\Gamma^2}{2}} L_{n+\delta-2}^{(0)}(\Gamma^2)$$

$$- \Gamma^2 \mathcal{N}_\delta \mathcal{N}_{\delta-2} \sum_{n=0}^{\infty} \frac{(\gamma^*)^{-2} |\gamma|^{2n+\delta}}{(n-2)!(n-1+\delta)!} e^{-\frac{\Gamma^2}{2}} L_{n+\delta-2}^{(1)}(\Gamma^2)$$

$$+ \frac{\Gamma^4}{4} \mathcal{N}_\delta \mathcal{N}_{\delta-2} \sum_{n=0}^{\infty} \frac{(\gamma^*)^{-2} |\gamma|^{2n+\delta}}{(n-2)!(n+\delta)!} e^{-\frac{\Gamma^2}{2}} L_{n+\delta-2}^{(2)}(\Gamma^2).$$

$$\langle a^\dagger a b^\dagger b \rangle = \frac{|\lambda|^2}{2} \left[(1 + |\langle \sigma_x \rangle_w|^2) P_{51} + (1 - |\langle \sigma_x \rangle_w|^2) P_{52} \right], \quad (\text{A5})$$

$$P_{51} = |\gamma|^2 + \frac{\Gamma^2}{4} \frac{|\gamma| I_{\delta+1}(2|\gamma|)}{I_\delta(2|\gamma|)},$$

$$P_{52} = \mathcal{N}_\delta^2 \sum_{n=0}^{\infty} \frac{|\gamma|^{2n+\delta}}{(n-1)!(n+\delta-1)!} e^{-\frac{\Gamma^2}{2}} L_{n+\delta}^{(0)}(\Gamma^2)$$

$$- \frac{\Gamma^2}{2} \mathcal{N}_\delta^2 \sum_{n=0}^{\infty} \frac{|\gamma|^{2n+\delta}}{(n-1)!(n+\delta)!} e^{-\frac{\Gamma^2}{2}} L_{n+\delta}^{(1)}(\Gamma^2)$$

$$+ \frac{\Gamma^2}{2} \mathcal{N}_\delta^2 \sum_{n=0}^{\infty} \frac{|\gamma|^{2n+\delta}}{(n-1)!(n+\delta)!} e^{-\frac{\Gamma^2}{2}} L_{n+\delta-1}^{(1)}(\Gamma^2)$$

$$+ \frac{\Gamma^2}{4} \mathcal{N}_\delta^2 \sum_{n=0}^{\infty} \frac{|\gamma|^{2n+\delta}}{(n-1)!(n+\delta)!} e^{-\frac{\Gamma^2}{2}} L_{n+\delta}^{(0)}(\Gamma^2).$$

$$\langle a^\dagger b \rangle = \frac{|\lambda|^2}{2} (1 - |\langle \sigma_x \rangle_w|^2) I_{11}, \quad (\text{A6})$$

$$I_{11} = \Gamma^2 \mathcal{N}_\delta \mathcal{N}_{\delta-1} \sum_{n=0}^{\infty} \frac{(\gamma^*)^{-1} |\gamma|^{2n+\delta}}{(n-1)!(n+\delta)!} e^{-\frac{\Gamma^2}{2}} L_{(n+\delta-1)}^{(2)}(\Gamma^2)$$

$$- \frac{\Gamma^2}{2} \mathcal{N}_\delta \mathcal{N}_{\delta-1} \sum_{n=0}^{\infty} \frac{(\gamma^*)^{-1} |\gamma|^{2n+\delta}}{(n-1)!(n+\delta)!} e^{-\frac{\Gamma^2}{2}} L_{(n+\delta-1)}^{(1)}(\Gamma^2).$$

$$\langle a^2 \rangle = \frac{|\lambda|^2}{2} \left[(1 + |\langle \sigma_x \rangle_w|^2) \frac{\Gamma^2}{4} + (1 - |\langle \sigma_x \rangle_w|^2) I_{21} \right], \quad (\text{A7})$$

$$\begin{aligned} I_{21} = & \Gamma^2 \mathcal{N}_\delta^2 \sum_{n=0}^{\infty} \frac{|\gamma|^{2n+\delta}}{n!(n+\delta)!} e^{-\frac{\Gamma^2}{2}} L_{(n+\delta-2)}^{(2)}(\Gamma^2) \\ & + \Gamma^2 \mathcal{N}_\delta^2 \sum_{n=0}^{\infty} \frac{|\gamma|^{2n+\delta}}{n!(n+\delta)!} e^{-\frac{\Gamma^2}{2}} L_{(n+\delta-1)}^{(1)}(\Gamma^2) \\ & + \frac{\Gamma^2}{4} \mathcal{N}_\delta^2 \sum_{n=0}^{\infty} \frac{|\gamma|^{2n+\delta}}{n!(n+\delta)!} e^{-\frac{\Gamma^2}{2}} L_{(n+\delta)}^{(0)}(\Gamma^2). \end{aligned}$$

$$\begin{aligned} \langle b^2 \rangle = & \frac{|\lambda|^2}{2} \left[(1 - |\langle \sigma_x \rangle_w|^2) I_{31} \right], \quad (\text{A8}) \\ I_{31} = & \mathcal{N}_\delta \mathcal{N}_{\delta-2} \sum_{n=0}^{\infty} \frac{(\gamma^*)^{-2} |\gamma|^{2n+\delta}}{(n-2)!(n+\delta)!} \Gamma^2 L_{n+\delta-2}^{(2)}(\Gamma^2) e^{-\frac{\Gamma^2}{2}}. \end{aligned}$$

$$\begin{aligned} \langle a \rangle = & \frac{|\lambda|^2}{2} [\Gamma \operatorname{Re} [\langle \sigma_x \rangle_w] - 2i \Im [\langle \sigma_x \rangle_w] I_{41}], \quad (\text{A9}) \\ I_{41} = & -\Gamma \mathcal{N}_\delta^2 \sum_{n=0}^{\infty} \frac{|\gamma|^{2n+\delta}}{n!(n+\delta)!} e^{-\frac{\Gamma^2}{2}} L_{(n+\delta-1)}^{(1)}(\Gamma^2) \\ & - \frac{\Gamma}{2} \mathcal{N}_\delta^2 \sum_{n=0}^{\infty} \frac{|\gamma|^{2n+\delta}}{n!(n+\delta)!} e^{-\frac{\Gamma^2}{2}} L_{(n+\delta)}^{(0)}(\Gamma^2). \end{aligned}$$

$$\begin{aligned} \langle b \rangle = & -i|\lambda|^2 \operatorname{Im} [\langle \sigma_x \rangle_w] I_{51}, \quad (\text{A10}) \\ I_{51} = & \Gamma \mathcal{N}_\delta \mathcal{N}_{\delta-1} \sum_{n=0}^{\infty} \frac{(\gamma^*)^{-1} |\gamma|^{2n+\delta}}{(n-1)!(n+\delta)!} e^{-\frac{\Gamma^2}{2}} L_{(n+\delta-1)}^{(1)}(\Gamma^2). \end{aligned}$$

$$\begin{aligned} \langle a^{\dagger 2} a^2 \rangle = & \frac{|\lambda|^2}{2} \left[(1 + |\langle \sigma_x \rangle_w|^2) K_{11} + (1 - |\langle \sigma_x \rangle_w|^2) K_{12} \right], \quad (\text{A11}) \\ K_{11} = & \frac{|\gamma|^2 I_{\delta-2}(2|\gamma|)}{I_\delta(2|\gamma|)} + \Gamma^2 \frac{|\gamma| I_{\delta-1}(2|\gamma|)}{I_\delta(2|\gamma|)} + \frac{\Gamma^4}{16}, \\ K_{12} = & \mathcal{N}_\delta^2 \sum_{n=0}^{\infty} \frac{|\gamma|^{2n+\delta}}{n!(n+\delta-2)!} e^{-\frac{\Gamma^2}{2}} L_{n+\delta}^{(0)}(\Gamma^2) \\ & - \Gamma \mathcal{N}_\delta^2 \sum_{n=0}^{\infty} \frac{|\gamma|^{2n+\delta}}{n!(n+\delta-1)!} e^{-\frac{\Gamma^2}{2}} \Gamma L_{(n+\delta)}^{(1)}(\Gamma^2) + \Gamma \mathcal{N}_\delta^2 \sum_{n=0}^{\infty} \frac{|\gamma|^{2n+\delta}}{n!(n+\delta)!} (n+\delta-1) e^{-\frac{\Gamma^2}{2}} \Gamma L_{(n+\delta-1)}^{(1)}(\Gamma^2) \\ & + \frac{\Gamma^2}{4} \mathcal{N}_\delta^2 \sum_{n=0}^{\infty} \frac{|\gamma|^{2n+\delta}}{n!(n+\delta)!} e^{-\frac{\Gamma^2}{2}} \Gamma^2 L_{(n+\delta)}^{(2)}(\Gamma^2) + \frac{\Gamma^2}{4} \mathcal{N}_\delta^2 \sum_{n=0}^{\infty} \frac{|\gamma|^{2n+\delta}}{n!(n+\delta)!} e^{-\frac{\Gamma^2}{2}} \Gamma^2 L_{(n+\delta-2)}^{(2)}(\Gamma^2) \\ & + \Gamma^2 \mathcal{N}_\delta^2 \sum_{n=0}^{\infty} \frac{|\gamma|^{2n+\delta}}{n!(n+\delta-1)!} e^{-\frac{\Gamma^2}{2}} L_{(n+\delta)}^{(0)}(\Gamma^2) - \frac{\Gamma^3}{4} \mathcal{N}_\delta^2 \sum_{n=0}^{\infty} \frac{|\gamma|^{2n+\delta}}{n!(n+\delta)!} e^{-\frac{\Gamma^2}{2}} \Gamma L_{(n+\delta)}^{(1)}(\Gamma^2) \\ & + \frac{\Gamma^3}{4} \mathcal{N}_\delta^2 \sum_{n=0}^{\infty} \frac{|\gamma|^{2n+\delta}}{n!(n+\delta)!} e^{-\frac{\Gamma^2}{2}} \Gamma L_{(n+\delta-1)}^{(1)}(\Gamma^2) + \frac{\Gamma^4}{16} \mathcal{N}_\delta^2 \sum_{n=0}^{\infty} \frac{|\gamma|^{2n+\delta}}{n!(n+\delta)!} e^{-\frac{\Gamma^2}{2}} L_{(n+\delta)}^{(0)}(\Gamma^2). \end{aligned}$$

$$\begin{aligned}
\langle b^{\dagger 2} b^2 \rangle &= \frac{|\lambda|^2}{2} \left[(1 + |\langle \sigma_x \rangle_w|^2) K_{21} + (1 - |\langle \sigma_x \rangle_w|^2) K_{22} \right], \\
K_{21} &= \frac{|\gamma|^2 I_{\delta+2}(2|\gamma|)}{I_{\delta}(2|\gamma|)}, \\
K_{22} &= \mathcal{N}_{\delta}^2 \sum_{n=0}^{\infty} \frac{|\gamma|^{2n+\delta}}{(n-2)!(n+\delta)!} e^{-\frac{\Gamma^2}{2}} L_{(n+\delta)}^{(0)}(\Gamma^2).
\end{aligned} \tag{A12}$$

The explicit expression of average fidelity F_{av} corresponding to the Eq. (41) is given by

$$\begin{aligned}
F_{av} = \frac{\mathcal{N}_{\delta}^2 \lambda^2}{8} \sum_{n=0}^{\infty} \sum_{m=0}^{\infty} \sum_{k=0}^{\infty} \sum_{l=0}^{\infty} & \frac{|\gamma|^{n+\delta/2} |\gamma|^{k+\delta/2}}{\sqrt{n!(n+\delta)!k!(k+\delta)!}} \frac{1}{\sqrt{n!m!l!k!}} \frac{1}{2^{m+k}} (m+k)! \delta_{m+k, n+l} \\
& \times \exp \left(-\left| \frac{\Gamma}{2} \right|^2 \right) (-1)^{\max(0, l-(\delta+k))} \sqrt{\frac{\min(l, \delta+k)! \min(m, \delta+n)!}{\max(l, \delta+k)! \max(m, \delta+n)!}} L_{\min(l, k+\delta)}^{|l-(k+\delta)|} \left(\left| \frac{\Gamma}{2} \right|^2 \right) L_{\min(m, n+\delta)}^{|m-(n+\delta)|} \left(\left| \frac{\Gamma}{2} \right|^2 \right) \\
& \times \left\{ |t_+|^2 \left(-\frac{\Gamma}{2} \right)^{|l-(k+\delta)|} \left(\frac{\Gamma}{2} \right)^{|m-(n+\delta)|} + t_+ t_-^* \left(\frac{\Gamma}{2} \right)^{|l-(k+\delta)|} \left(\frac{\Gamma}{2} \right)^{|m-(n+\delta)|} \right. \\
& \left. + t_+^* t_- \left(-\frac{\Gamma}{2} \right)^{|l-(k+\delta)|} \left(-\frac{\Gamma}{2} \right)^{|m-(n+\delta)|} + |t_-|^2 \left(\frac{\Gamma}{2} \right)^{|l-(k+\delta)|} \left(-\frac{\Gamma}{2} \right)^{|m-(n+\delta)|} \right\}
\end{aligned} \tag{A13}$$

[1] A. I. Lvovsky, P. Grangier, A. Ourjoumtsev, V. Parigi, M. Sasaki, and R. Tualle-Brouri, (2020), [arXiv:2006.16985 \[quant-ph\]](https://arxiv.org/abs/2006.16985).

[2] M. Walschaers, Non-Gaussian Quantum States and Where to Find Them, *PRX Quantum* **2**, 030204 (2021).

[3] W. Asavanant and A. Furusawa, Multipartite continuous-variable optical quantum entanglement: Generation and application, *Phys. Rev. A* **109**, 040101 (2024).

[4] C. Wang, Y. Y. Gao, P. Reinhold, R. W. Heeres, N. Ofek, K. Chou, C. Axline, M. Reagor, J. Blumoff, K. M. Sliwa, L. Frunzio, S. M. Girvin, L. Jiang, M. Mirrahimi, M. H. Devoret, and R. J. Schoelkopf, A Schrödinger cat living in two boxes, *Science* **352**, 1087 (2016).

[5] I. Afek, O. Ambar, and Y. Silberberg, High-NOON States by Mixing Quantum and Classical Light, *Science* **328**, 879 (2010).

[6] H. Wang, M. Mariantoni, R. C. Bialczak, M. Lenander, E. Lucero, M. Neeley, A. D. O'Connell, D. Sank, M. Weides, J. Wenner, T. Yamamoto, Y. Yin, J. Zhao, J. M. Martinis, and A. N. Cleland, Deterministic Entanglement of Photons in Two Superconducting Microwave Resonators, *Phys. Rev. Lett.* **106**, 060401 (2011).

[7] L. Dao-ming, Quantum Properties of Single-Mode Squeezing and Two-Mode Squeezing Repeated Role Two-Mode Vacuum State, *Int. J. Theor. Phys.* **54**, 2289 (2015).

[8] M. Riabinin, P. R. Sharapova, T. J. Bartley, and T. Meier, Generating two-mode squeezing with multimode measurement-induced nonlinearity, *J. Phys. Commun.* **5**, 045002 (2021).

[9] G. S. Agarwal, Generation of Pair Coherent States and Squeezing via the Competition of Four-Wave Mixing and Amplified Spontaneous Emission, *Phys. Rev. Lett.* **57**, 827 (1986).

[10] K. Tara and G. S. Agarwal, Einstein-Podolsky-Rosen paradox for continuous variables using radiation fields in the pair-coherent state, *Phys. Rev. A* **50**, 2870 (1994).

[11] A. Gábris and G. S. Agarwal, QUANTUM TELEPORTATION WITH PAIR-COHERENT STATES, *Int. J. Quantum Inf.* **05**, 17 (2007).

[12] C. Zhou, W. Bao, and X. Fu, Decoy-state quantum key distribution for the heralded pair coherent state photon source with intensity fluctuations, *Sci. China Inf. Sci.* **53**, 2485 (2010).

[13] K. P. Seshadreesan, J. P. Dowling, and G. S. Agarwal, Non-Gaussian entangled states and quantum teleportation of Schrödinger-cat states*, *Phys. Scr.* **90**, 074029 (2015).

[14] H. Vahlbruch, M. Mehmet, K. Danzmann, and R. Schnabel, Detection of 15 dB Squeezed States of Light and their Application for the Absolute Calibration of Photoelectric Quantum Efficiency, *Phys. Rev. Lett.* **117**, 110801 (2016).

[15] L. Wang and S. Zhao, Round-robin differential-phase-shift quantum key distribution with heralded pair-coherent sources, *Quantum Inf. Process.* **16**, 100 (2017).

[16] F. Acernese, Agathos, and et al. (Virgo Collaboration), Increasing the Astrophysical Reach of the Advanced Virgo Detector via the Application of Squeezed Vacuum States of Light, *Phys. Rev. Lett.* **123**, 231108 (2019).

[17] T. Q. Dat, Entanglement, Nonlocality, Quantum Teleportation of Two-mode Non-Gaussian States with Multiphoton Quantum Catalysis, *Int. J. Theor. Phys.* **62**, 41 (2023).

[18] V. Roman-Rodriguez, D. Fainsin, G. L. Zanin, N. Treps, E. Diamanti, and V. Parigi, Multimode squeezed state for reconfigurable quantum networks at telecommunication wavelengths, *Phys. Rev. Res.* **6**, 043113 (2024).

[19] L. Hong, Statistical properties of photon-added and photon-subtracted two-mode squeezed vacuum state, *Phys. Lett. A* **264**, 265 (1999).

[20] L. Hong and G. Guang-can, Nonclassical properties of photon-added pair coherent states, *Acta Phys. Sinica (Overseas Edition)* **8**, 577 (1999).

[21] A. Kitagawa, M. Takeoka, M. Sasaki, and A. Chefles, Entanglement evaluation of non-Gaussian states generated by photon subtraction from squeezed states, *Phys. Rev. A* **73**, 042310 (2006).

[22] A. Biswas and G. S. Agarwal, Nonclassicality and decoherence of photon-subtracted squeezed states, *Phys. Rev. A* **75**, 032104 (2007).

[23] H.-C. Yuan, X.-X. Xu, and H.-Y. Fan, Statistical Properties of the Generalized Photon-Added Pair Coherent State, *Int. J. Theor. Phys.* **48**, 3596 (2009).

[24] D. M. Truong, H. T. X. Nguyen, and A. B. Nguyen, Sum Squeezing, Difference Squeezing, Higher-Order Antibunching and Entanglement of Two-Mode Photon-Added Displaced Squeezed States, *Int. J. Theor. Phys.* **53**, 899 (2014).

[25] N. T. X. Hoai and T. M. Duc, Nonclassical properties and teleportation in the two-mode photon-added displaced squeezed states, *Int. J. Mod. Phys. B* **30**, 1650032 (2016).

[26] H.-C. Yuan, X.-X. Xu, and Y.-J. Xu, Generating two-variable Hermite polynomial excited squeezed vacuum states by conditional measurement on beam splitters, *Optik* **172**, 1034 (2018).

[27] D.-M. Lu, Quantum Properties of the State via Operation of Superposition of Photon Subtraction Two Times and Photon Addition Two Times on Two Modes Squeezing Vacuum State, *Int. J. Theor. Phys.* **57**, 2767 (2018).

[28] T. M. Duc, D. H. Dinh, and T. Q. Dat, Higher-order nonclassical properties of nonlinear charge pair cat states, *J. Phys. B* **53**, 025402 (2019).

[29] T. M. Duc, T. Q. Dat, and H. S. Chuong, Quantum entanglement and teleportation in superposition of multiple-photon-added two-mode squeezed vacuum state, *Int. J. Mod. Phys. B* **34**, 2050223 (2020).

[30] D. M. Truong, C. S. Ho, and D. Q. Tran, Detecting nonclassicality and non-Gaussianity by the Wigner function and quantum teleportation in photon-added-and-subtracted two modes pair coherent state, *J. Comput. Electron.* **20**, 2124 (2021).

[31] H. S. Chuong and T. M. Duc, Enhancement of non-Gaussianity and nonclassicality of pair coherent states by superposition of photon addition and subtraction, *J. Phys. B* **56**, 205401 (2023).

[32] V. Parigi, A. Zavatta, M. Kim, and M. Bellini, Probing Quantum Commutation Rules by Addition and Subtraction of Single Photons to/from a Light Field, *Science* **317**, 1890 (2007).

[33] K. Sanaka, K. J. Resch, and A. Zeilinger, Filtering Out Photonic Fock States, *Phys. Rev. Lett.* **96**, 083601 (2006).

[34] H. M. Wiseman and G. J. Milburn, *Quantum Measurement and Control* (Cambridge University Press, Cambridge, England, 2014).

[35] Y. Aharonov, D. Z. Albert, and L. Vaidman, How the result of a measurement of a component of the spin of a spin-1/2 particle can turn out to be 100, *Phys. Rev. Lett.* **60**, 1351 (1988).

[36] B. Tamir and E. Cohen, Introduction to Weak Measurements and Weak Values, *Quanta* **2**, 7 (2013).

[37] B. Svensson, Pedagogical Review of Quantum Measurement Theory with an Emphasis on Weak Measurements, *Quanta* **2**, 18 (2013).

[38] J. Harris, R. W. Boyd, and J. S. Lundeen, Weak Value Amplification Can Outperform Conventional Measurement in the Presence of Detector Saturation, *Phys. Rev. Lett.* **118**, 070802 (2017).

[39] A. G. Kofman, S. Ashhab, and F. Nori, Nonperturbative theory of weak pre- and post-selected measurements, *Phys. Rep.* **520**, 43 (2012), nonperturbative theory of weak pre- and post-selected measurements.

[40] J. Dressel, M. Malik, F. M. Miatto, A. N. Jordan, and R. W. Boyd, Colloquium: Understanding quantum weak values: Basics and applications, *Rev. Mod. Phys.* **86**, 307 (2014).

[41] Q. Hu, T. Yusufu, and Y. Turek, Quantum state engineering using weak measurements, *Phys. Rev. A* **105**, 022608 (2022).

[42] W. J. Xu, T. Yusufu, and Y. Turek, Studying the squeezing effect and phase-space distribution of a single-photon-added coherent state using a postselected von Neumann measurement, *Phys. Rev. A* **105**, 022210 (2022).

[43] Y. Turek, A. Islam, and A. Abiliz, Single-photon-added coherent state-based measurement transition and its advantages in precision measurement, *Eur. Phys. J. Plus* **138**, 72 (2023).

[44] G. S. Agarwal, Nonclassical statistics of fields in pair coherent states, *J. Opt. Soc. Am. B* **5**, 1940 (1988).

[45] S.-C. Gou, J. Steinbach, and P. L. Knight, Vibrational pair cat states, *Phys. Rev. A* **54**, 4315 (1996).

[46] S.-B. Zheng, Generation of pair coherent and cat states for the motion of two trapped ions, *Czechoslov. J. Phys.* **52**, 713 (2002).

[47] A.-S. Obada and E. Khalil, Generation and some nonclassical properties of a finite dimensional pair coherent state, *Opt. Commun.* **260**, 19 (2006).

[48] Y.-L. Dong, X.-B. Zou, and G.-C. Guo, Generation of pair coherent state using weak cross-Kerr media, *Phys. Lett. A* **372**, 5677 (2008).

[49] C. C. Gerry, J. Mimih, and R. Birrittella, State-projective scheme for generating pair coherent states in traveling-wave optical fields, *Phys. Rev. A* **84**, 023810 (2011).

[50] J. M. Gertler, S. van Geldern, S. Shirol, L. Jiang, and C. Wang, Experimental Realization and Characterization of Stabilized Pair-Coherent States, *PRX Quantum* **4**, 020319 (2023).

[51] H. Jeon, J. Kang, J. Kim, W. Choi, K. Kim, and T. Kim, Experimental realization of entangled coherent states in two-dimensional harmonic oscillators of a trapped ion, *Sci. Rep.* **14**, 6847 (2024).

[52] M. D. Truong, Q. D. Tran, and P. D. Le, Improved experimental scheme for the generation of pair coherent state in traveling-wave optical fields, *Laser Physics Letters* **21**, 115207 (2024).

[53] C. T. Lee, Many-photon antibunching in generalized pair

coherent states, *Phys. Rev. A* **41**, 1569 (1990).

[54] A.-S. F. Obada, M. M. A. Ahmed, and S. Sanad, Non-classical properties for $SU(1, 1)$ pair coherent states, *J. Phys. Commun.* **4**, 015008 (2020).

[55] A. GÁBRIS and G. S. AGARWAL, QUANTUM TELEPORTATION WITH PAIR-COHERENT STATES, *Int. J. Quantum Inf.* **05**, 17 (2007).

[56] V. V. Albert, S. O. Mundhada, A. Grimm, S. Touzard, M. H. Devoret, and L. Jiang, Pair-cat codes: autonomous error-correction with low-order nonlinearity, *Quantum Sci. Technol.* **4**, 035007 (2019).

[57] Y.-X. Gong, Quantum interferometric lithography with pair-coherent states, *Phys. Rev. A* **88**, 043841 (2013).

[58] V. Giovannetti, S. Lloyd, and L. Maccone, Quantum Metrology, *Phys. Rev. Lett.* **96**, 010401 (2006).

[59] B. A. Nguyen, Quantum dialogue, *Physics Letters A* **328**, 6 (2004).

[60] Y. Turek, H. Kobayashi, T. Akutsu, C.-P. Sun, and Y. Shikano, Post-selected von Neumann measurement with Hermite–Gaussian and Laguerre–Gaussian pointer states, *New Journal of Physics* **17**, 083029 (2015).

[61] Y. Turek, W. Maimaiti, Y. Shikano, C.-P. Sun, and M. Al-Amri, Advantages of nonclassical pointer states in postselected weak measurements, *Phys. Rev. A* **92**, 022109 (2015).

[62] U. Andersen, G. Leuchs, and C. Silberhorn, Continuous-variable Quantum Inf. Process., *Laser Photonics Rev.* **4**, 337 (2010).

[63] R. Schnabel, Squeezed states of light and their applications in laser interferometers, *Phys. Rep.* **684**, 1 (2017), squeezed states of light and their applications in laser interferometers.

[64] G. Agarwal, *Quantum Optics* (Cambridge University Press, Cambridge, England, 2013).

[65] M. Hillery, Sum and difference squeezing of the electromagnetic field, *Phys. Rev. A* **40**, 3147 (1989).

[66] W. K. Lai, V. Buek, and P. L. Knight, Dynamics of a three-level atom in a two-mode squeezed vacuum, *Phys. Rev. A* **44**, 6043 (1991).

[67] A. M. Bhargav, A. Wahid, S. Das, and V. G. Achanta, Second-Order Correlation Measurement for Single-Photon Metrology, *MAPAN* **38**, 997 (2023).

[68] H. Paul, Photon antibunching, *Rev. Mod. Phys.* **54**, 1061 (1982).

[69] B. Lounis and M. Orrit, Single-photon sources, *Rep. Prog. Phys.* **68**, 1129 (2005).

[70] G. S. Agarwal and A. Biswas, Quantitative measures of entanglement in pair-coherent states, *J. Opt. B: Quantum Semiclass. Opt.* **7**, 350 (2005).

[71] M. Hillery and M. S. Zubairy, Entanglement Conditions for Two-Mode States, *Phys. Rev. Lett.* **96**, 050503 (2006).

[72] F. Li, T. Li, and G. S. Agarwal, Experimental study of decoherence of the two-mode squeezed vacuum state via second harmonic generation, *Phys. Rev. Res.* **3**, 033095 (2021).

[73] L.-M. Duan, G. Giedke, J. I. Cirac, and P. Zoller, Inseparability Criterion for Continuous Variable Systems, *Phys. Rev. Lett.* **84**, 2722 (2000).

[74] G. Ren, W. hai Zhang, and Y. jun Xu, Nonclassical properties of two-mode squeezing-enhanced vacuum state, *Physica A* **520**, 106 (2019).

[75] L. Vaidman, Teleportation of quantum states, *Phys. Rev. A* **49**, 1473 (1994).

[76] S. L. Braunstein and H. J. Kimble, Teleportation of Continuous Quantum Variables, *Phys. Rev. Lett.* **80**, 869 (1998).

[77] A. Furusawa, J. L. Sørensen, S. L. Braunstein, C. A. Fuchs, H. J. Kimble, and E. S. Polzik, Unconditional Quantum Teleportation, *Science* **282**, 706 (1998).

[78] H. F. Hofmann, T. Ide, T. Kobayashi, and A. Furusawa, Fidelity and information in the quantum teleportation of continuous variables, *Phys. Rev. A* **62**, 062304 (2000).

[79] S. Wu and M. Żukowski, Feasible Optical Weak Measurements of Complementary Observables via a Single Hamiltonian, *Phys. Rev. Lett.* **108**, 080403 (2012).

[80] Y. Liu, L. Qin, and X.-Q. Li, Fisher information analysis on weak-value-amplification metrology using optical coherent states, *Phys. Rev. A* **106**, 022619 (2022).

[81] P. Kok, W. J. Munro, K. Nemoto, T. C. Ralph, J. P. Dowling, and G. J. Milburn, Linear optical quantum computing with photonic qubits, *Rev. Mod. Phys.* **79**, 135 (2007).

[82] M. D. Truong and Q. D. Tran, Enhancing quantum features and teleportation fidelity of two-mode non-Gaussian states using conditional measurements, *Laser Phys. Lett.* **21**, 035205 (2024).

[83] N. Horiuchi, Single-photon subtraction, *Nat. Photonics* **11**, 532 (2017).

[84] P. B. Dixon, D. J. Starling, A. N. Jordan, and J. C. Howell, Ultrasensitive Beam Deflection Measurement via Interferometric Weak Value Amplification, *Phys. Rev. Lett.* **102**, 173601 (2009).

[85] Y.-T. Wang, J.-S. Tang, G. Hu, J. Wang, S. Yu, Z.-Q. Zhou, Z.-D. Cheng, J.-S. Xu, S.-Z. Fang, Q.-L. Wu, C.-F. Li, and G.-C. Guo, Experimental Demonstration of Higher Precision Weak-Value-Based Metrology Using Power Recycling, *Phys. Rev. Lett.* **117**, 230801 (2016).

[86] X.-Y. Xu, Y. Kedem, K. Sun, L. Vaidman, C.-F. Li, and G.-C. Guo, Phase Estimation with Weak Measurement Using a White Light Source, *Phys. Rev. Lett.* **111**, 033604 (2013).

[87] J. Zhu, Z. Li, Y. Liu, Y. Ye, Q. Ti, Z. Zhang, and F. Gao, Weak measurement with the peak-contrast-ratio pointer, *Phys. Rev. A* **103**, 032212 (2021).

[88] C.-W. Wu, J. Zhang, Y. Xie, B.-Q. Ou, T. Chen, W. Wu, and P.-X. Chen, Scheme and experimental demonstration of fully atomic weak-value amplification, *Phys. Rev. A* **100**, 062111 (2019).

[89] Y. Pan, J. Zhang, E. Cohen, C.-W. Wu, P.-X. Chen, and N. Davidson, Weak-to-strong transition of quantum measurement in a trapped-ion system, *Nat. Phys.* **16**, 1206 (2020).

[90] W. Su, M. Zhang, C. Wu, Y. Xie, H. Hu, T. Chen, T. Zhan, B. Ou, W. Wu, J. Zhang, and P. Chen, Experimental measurement for the expectation value of the product of two noncommuting observables via weak measurement in a trapped-ion system, *Phys. Rev. A* **108**, 042601 (2023).

[91] C. Wu, H. Hu, J. Zhang, W. Su, M. Zhang, T. Zhan, Q. Qin, W. Wu, and P. Chen, Experimental verification of quantum contextuality using a weak measurement in a single trapped ion, *Phys. Rev. A* **109**, 032211 (2024).

[92] Y.-S. Ra, A. Dufour, M. Walschaers, C. Jacquard, T. Michel, C. Fabre, and N. Treps, Non-Gaussian quantum states of a multimode light field, *Nat. Phys.* **16**, 144 (2020).